NASA Contractor Report 195457

Method for Extracting Forward Acoustic Wave Components from Rotating Microphone Measurements in the Inlets of Turbofan Engines

D. E. Cicon
United Technologies Corporation
Pratt and Whitney
East Hartford, Connecticut

T. G. Sofrin
Consultant
Newington, Connecticut

April 1995

TABLE OF CONTENTS

Page

SUMMARY

In previous work by Pratt and Whitney and NASA–Lewis, a rotating microphone data acquisition/ reduction system was developed to resolve acoustic pressures in an engine inlet plane into constituent harmonics of blade passing frequency and circumferential and radial mode orders. Although this system met its design objectives, it had no means of distinguishing forward (upstream–going) waves from waves that might be reflected downstream from the engine inlet.

This report describes a procedure for enhancing the use of the basic rotating microphone system so as to determine the forward propagating mode components of the acoustic field in the inlet duct at the microphone plane for more accurate prediction of far–field radiation patterns. In addition, a modification was developed to obtain, from the same microphone readings, the forward acoustic modes generated at the fan face, which is generally some distance downstream of the microphone plane. Both these procedures employ computer–simulated calibrations of sound propagation in the inlet duct, based upon a finite element radiation code.

These enhancement procedures were applied to previously obtained rotating microphone data for the 17–inch ADP fan. The forward mode components at the microphone plane were obtained and were used to compute corresponding far–field directivities. In–duct mode amplitudes and far field directivities were compared for the basic and enhanced systems. For the four cases evaluated, the enhanced data reduction scheme made only a small difference in predicted noise levels. The reason for this negative result is that, while some modes were near cutoff, the microphone array was not located near a pressure extreme in the standing wave pattern.

To demonstrate that the enhanced data reduction scheme is needed under conditions where a mode might be near cutoff, an analytical simulation was performed using an acoustic field inside and outside an inlet generated by a finite element acoustic code. The basic and enhanced methods for projecting internal measurements to the far field were applied, assuming various locations for the rotating microphone plane. Depending on mic plane location, far field predictions using the basic data reduction scheme varied over a range of 12 dB. When the enhanced scheme was applied, the far field directivity patterns collapsed into a ± 0.5 dB band. The success of this demonstration indicated that the reflected wave effect can introduce large error into estimates of the outgoing modes from the fan. It also indicated that the new scheme can be very effective in eliminating the reflected wave contamination.

The second main task of the program involved finding the forward wave modes generated at the fan face in terms of the same total radial mode structure measured at the microphone plane (nearer to the inlet). This was not as simple a matter as before; initial calculations gave obviously wrong results. To resolve this problem, a set of computer–simulated sensitivity studies was made that showed the effects of small measurement errors. These indicated that, for the spacing between fan and microphone planes used in the ADP tests, the enhancement procedure could be applied successfully only to the propagating radial modes. With this limitation, satisfactory predictions of the fan modes were obtained using the test data.

The sensitivity studies also led to recommendations for future design and use of the rotating microphone system on other fan configurations.

INTRODUCTION

The rotating microphone system (Reference 1) was designed to provide detailed information on the circumferential–radial mode structure of the acoustic field in inlets of turbofan engines and to obtain this information using a number of microphone elements that is dramatically smaller than would be needed with fixed microphone arrays.

The concept was applied to a rotating rake which provided 9 radial microphone locations. The microphone signals were frequency–analyzed with a very high resolution Fourier transform. Each frequency thus obtained could be uniquely associated with the spinning mode index (m); this separation is made possible by the (low) rotation speed of the microphone array (Reference 1). For each spinning mode sensed by the microphones, the associated radial mode structure is obtained by least squares fitting the 9 complex microphone pressures to the first 4 associated radial mode (Bessel) functions.

In 1991 rotating microphone tests were run on the 17–inch diameter Advanced Ducted Propulsor (ADP) rig in a wind tunnel at Lewis Research Center. Descriptions of the test procedures and rotating microphone usage are given in References 2–4.

These tests provided the circumferential and radial mode structure of the total acoustic pressure in the inlet at the plane of microphone location, and were also used as a basis for computing the associated far field radiation directivity pattterns for selected modes. However, the pressure measured by the rotating rake consists of two components: The primary component is the forward going wave generated by the fan, p^+, but there is also present a backward wave reflected from the mouth of the inlet, p^-. Only the p^+ forward wave generates the outside radiation field, and use of the total measured pressure, $p = p^+ + p^-$, will introduce error if p^- is significant.

For the measured cases which were studied, far field differences were not large. In an effort to determine if there are conditions for which large differences can exist between the basic and enhanced systems, an analytical simulation was run with the results shown in Figure 1. The geometry used for the simulation was the ADP long inlet. At a speed of 7500 rpm, Blade Passing Frequency propagates in the 6,0 mode which is just slightly cut on. (Cutoff ratio $\xi = 1.12$ at the fan face and 1.07 at plane M.) All other modes are well cut off and can be neglected. The noise field within the duct was predicted assuming a unit amplitude input at the fan face for the single propagating mode and is shown in the top panel of Figure 1. Following this, the noise field was interpolated to obtain pressure data as though measured by a microphone array for the three other axial locations indicated in the figure. The enhanced system was then used to determine the p^+ levels at each array location. Far field estimates based on both p and p^+ at the source and the three other axial locations were computed and are shown in Figure 1. Differences of about 12 dB can be seen for the data estimated from p (center panel) while the predictions based on p^+ (bottom panel) agree to within about 0.5 dB. Near a pressure maximum such as location H, the p levels can approach $p^+ + 6$ dB. Near a node such as location G, the total p can become very small compared to p^+, resulting in a very large change in predicted far field levels.

The remainder of this report presents a derivation of the equations for the enhanced system plus applications to rotating mic data from the 17 inch ADP model.

TASK DESCRIPTION – ENHANCED ROTATING MICROPHONE METHODS

The procedure for enhancing measured microphone outputs involves using Eversman's radiation code (Reference 5). By using finite element numerical methods, this computes the acoustic field in the duct and the far field that results from known forward wave inputs. Inside the inlet, this field is considered to be the sum of both forward–going and reflected waves.

The task was divided into two parts for convenience:

Application 1 – Improved method to predict far field noise from rotating microphone data.

This application has been described in the Introduction. It consists of devising a way for extracting the forward wave component, p^+, from the total measured pressure at the rotating microphone plane and using this quantity to obtain an improved prediction of the far field.

Application 2 – Source diagnosis method

It turns out that the basic methodology involved in Application 1 can be modified in a fairly obvious way to attack another important problem in fan noise measurement and interpretation. This is the matter of determining what forward modes the fan is generating as a source. This information is needed to verify theories about fan noise generating processes and their prediction. If the rotating microphone could be placed close to the fan leading edge plane, the methods of Application 1 would suffice. However, mechanical constraints prevent this extreme positioning. Instead, a way must be found to use microphone data measured in a plane nearer to the inlet to infer the source characteristics.

ANALYSIS

Basic Relations

In any plane normal to the fan duct axis the periodic acoustic pressure is represented here for simplicity as the real part of

$$P(\theta, r, t) = \sum_{m=-\infty}^{\infty} \sum_{\mu=0}^{\infty} C_{m\mu} \Psi_{m\mu}(r) \, \exp i(m\theta - \omega t) \qquad (1)$$

where $\Psi_{m\mu}(r) = J_m(k_{m\mu}r) + Q_{m\mu}Y_m(k_{m\mu}r)$, and the eigenvalues $k_{m\mu}$ and $Q_{m\mu}$ are evaluated for the appropriate hub and tip boundary conditions at that plane.

Operation of the rotating microphone system automatically separates frequency (ω = BPF, 2BPF, etc.) and circumferential mode wavenumber, m. Then for any m and ω, Equation (1) reduces to

$$P(r) = \sum_{\mu=0}^{\infty} C_{m\mu} \Psi_{m\mu}(r) \qquad (2)$$

Values of the complex coefficients, $C_{m\mu}$, are obtained from measured values of P(r) taken from the microphone outputs at a number of radial locations (9 in this program). A least squares fit of Equation (2) to the 9 values of P(r) serves to give values of $C_{m\mu}$. While, in principle, it is possible to obtain the first 9 coefficients from 9 points, it is well known, e.g. (Reference 6), that slight measurement and/or computation errors can render the results useless. By fitting Equation (2) to only about one–half the maximum number of modes, more reliable results are obtained. For this reason a fit to the first 4 radial modes has been used in this program. If, in other applications, a larger number of modes are known to be propagating, provision must be made in advance to employ a suitably larger number of microphone locations.

In the following work it will simplify and clarify matters if we make the following change in notation: With the understanding that m and ω are known and fixed, a radial mode can be identified by the coefficient $C_{m\mu}$: this can further be abbreviated by replacing $C_{m\mu}$ by the symbol p_μ.

$$\text{Complex coefficient of } \mu\text{-th radial mode} = p_\mu \ (= C_{m\mu}) \qquad (3)$$

If several radial modes are present in a transverse plane, the collection can be represented simply by a vector or column matrix:

For example, with 3 modes

$$p = \begin{bmatrix} p_1 \\ p_2 \\ p_3 \end{bmatrix} \qquad (4)$$

p represents the measured total pressure field in a transverse plane and is extracted from the data as has previously been described. It is the result of waves traveling upstream from the fan and reflected waves traveling downstream from the inlet, or p^+ and p^- waves:

$$p = p^+ + p^-,\qquad\qquad(5)$$

that is

$$\begin{bmatrix} p_1 \\ p_2 \\ p_3 \end{bmatrix} = \begin{bmatrix} p_1^+ \\ p_2^+ \\ p_3^+ \end{bmatrix} + \begin{bmatrix} p_1^- \\ p_2^- \\ p_3^- \end{bmatrix}$$

for 3 modes.

The general objective of this investigation is to separate the measured total mode pressure, p, into its forward and backward wave components, p^+ and p^-.

The key to solution lies in "calibrating" the duct with a sequence of _unit_ forward wave inputs, p^+, and finding the resulting outputs, p. These calibrations will be made by use of the radiation code as explained below.

The result of the calibration may be expressed as the linear relation

$$p = D\,p^+,\qquad\qquad(6)$$

where elements of the square matrix, D, are now considered known.

The solution is obtained by inverting (6) to give the desired forward waves, p^+, in terms of the measured waves, p:

$$p+ = D^{-1}\,p.\qquad\qquad(7)$$

The reflected waves can be obtained from

$$p^- = p - p+ = (I - D^{-1})\,p.\qquad\qquad(8)$$

Eversman's code is applicable since it gives p everywhere in the acoustic field for specified values of p^+ input at the boundary of his computational domain, a plane in the inlet.

Details of the calibration procedure and its use in processsing measured data, p, will now be presented, first for Application 1.

Analysis for Application 1 – Improved Method to Predict Far Field Noise from Rotating Microphone Data :

In previous work the measured microphone mode structure has been used as input to the radiation code to compute far field directivity. This application requires that the total mode structure at the microphone be resolved into forward and backward waves, and that only the forward component be used to compute far field.

To signify that the microphone plane specifically is involved, subscripts M are appended to Equations (5), (6), and (7), giving:

$$p_M = p_M^+ + p_M^- \qquad (9)$$

$$p_M = D_{MM} \; p_M^+ \qquad (10)$$

$$p_M^+ = D_{MM}^{-1} \; p_M \qquad (11)$$

These equations are illustrated in Figure 2.

To find the elements of D_{MM}, the radiation code is set up with the origin of the mesh system located at the microphone plane. This mesh system is shown in Figure 3. The code computes values of the (total) pressure, p, in the inlet for any specified p_M^+ mode structure.

To "calibrate" the duct, a sequence of unit p_M^+, modes is applied at the mesh origin and the resulting total pressures are computed at points in the microphone plane. These pressures are converted into radial mode constituents by least squares methods. (43 mesh points were used in the microphone plane, so that the least squares procedure used in computer simulated calibration will determine the first few modes to a high degree of accuracy.)

Each unit mode vector, p_M^+, will produce output mode values, p_M, which constitute the elements in the corresponding columns of the D–matrix. Figure 4 illustrates this calibration procedure, using a 3–mode system for convenience.

With the D–matrix in hand, it is then possible to extract the forward wave components from rotating microphone data taken in tests on the 17–inch ADP rig. Details of these procedures and results are described in a later section of this report.

Analysis for Application 2 – Source Diagnosis Method

In this application the same microphone readings, p_M, are to be used to infer the forward mode structure generated at the fan face. This information will be of use in validating theoretical models for noise generation by rotor–stator interaction.

The relation between microphone measured modes, p_M, and the fan source forward modes, denoted here by p_F^+, will have a linear structure given by the (different) matrix equation

$$p_M = D_{MF} \; p_F^+ \qquad\qquad (12)$$

Figure 5 shows this relation for Application 2.

A new calibration sequence of unit p_F^+ modes must be used to establish values of the D_{MF} matrix elements by setting up the radiation code mesh origin back at the fan face. This mesh is shown in Figure 6.

The calibration procedure for Application 2 is shown in Figure 7. (This procedure may be easier to visualize, since the forward wave input, p_F^+, and the total pressure output, p_M, are located at 2 distinct places in the duct.)

With the elements of D_{MF} in hand, the desired fan mode structure is obtained by inversion:

$$p_F^+ = D_{MF}^{-1} \; p_M \qquad\qquad (13)$$

Procedures and results involved in Application 2 are described in the next section.

PROCEDURES AND RESULTS

The enhancement procedures described in the Analysis section were applied to the geometry of the 17–inch ADP rig incorporating the so–called "medium inlet" or "mid–inlet". See Figure 8. Data from the rotating microphone array were extracted at fan speeds of 9,600 rpm, 11,400 rpm, and 12,000 rpm. For the configuration incorporating a 22–vane stator with the 16–blade rotor, the inter-action tone has a circumferential mode m=–6 (=16 – 22) for the fundamental blade–passage order, BPF. Additionally, at 9,600 rpm 2BPF was analyzed for m=10 (=32–22). Radial mode structures were obtained by NASA LeRC, using a least–squares fit of 4 radial modes to the data at 9 radial microphone locations. In Figures 9 through 12 the demarcations between propagating and decaying modes are indicated.

Application 1

This application consists of extracting the forward mode component vector, p_M^+, from the measured (total) microphone mode structure, (p_M), for the test conditions described above. This p_M^+ structure was then used to compute the far field and to compare results with those obtained using p_M as a source.

The enhancement procedure involves obtaining the matrix D_{MM} in Equation 10 by computer simu-lated calibrations and applying it to the data, p_M. The calibrations were made by using the radiation code with the source (input boundary) located in the microphone plane. The finite element grid is shown in Figure 3.

Figures 9, 10, and 11 show the amplitudes of the 4 components of p_M^+, together with p_M, and the far field directivity for the sum of the complex components. These figures are for BPF at 9,600, 11,400, and 12,000 fan rpm. Figure 12 presents corresponding information for 2BPF at 9,600 rpm.

Some observations may be made about these 4 figures. For the conditions presented, the differences between mode amplitudes, p_M^+ and p_M, are less than 4 dB. In the majority of cases the magnitude of p_M is greater than the forward wave, p_M^+.

In Figure 9 the directivity curves are indistinguishable. For this case there is only one propagating mode which is well cut on at this speed so that the reflected wave is practically zero. Since the for-ward mode component, p_M^+, is nearly equal to the total mode amplitude, p_M, this result is not surpris-ing.

More significant differences can be seen in Figure 10, where two radial orders propagate and the p_M and p_M^+ mode amplitudes for the μ=1 radial order differ by about 3 dB at radiation angles be-tween 60 degrees and 90 degrees. At this speed the μ=1 mode has a cutoff ratio of about 1.07 so that some reflection of this mode might be expected. At about 40 degrees where the major lobe peaks for the μ=0 mode, the p_M^+ directivity pattern is slightly lower than the pattern generated using p_M.

The difference is similar to the difference between the p_M and the p_M^+ mode amplitudes for the $\mu=0$ mode. At larger angles, where higher order radial modes have their maximum amplitudes, the difference between the directivity curves is similar to the difference in the $\mu=1$ mode amplitudes.

At 12,000 rpm, Figure 11, the propagating modes are similar in amplitude so that little difference in directivities would be expected and this is seen to be the case. A larger difference is seen betweeen the $\mu=2$ mode amplitudes, but, since these are cut off, no differences would be expected to occur in the far field.

Three radial modes propagate for the case shown in Figure 12. The $\mu=2$ mode has a cutoff ratio of about 1.06 and appears to have a significant reflected component. This is likely the cause of the directivity curve differences above 50 degrees. Below 50 degrees, three modes with similar amplitudes combine and their relative phasing is probably responsible for the larger directivity levels for the p_M^+ modes even though all three propagating mode magnitudes are lower.

From these sample results it seems that far field directivity can be significantly changed if one of the modes is near cutoff. If few modes are present, differences will probably be observed at angles larger than that of the main lobe of the lowest order mode. Also, for airplane noise calculations, constant radius data is extrapolated to constant sideline distances, giving the results at larger angles somewhat more importance than is indicated here. As the number of modes increases, however, the effect of substituting p_M^+ mode amplitudes for p_M mode amplitudes will probably be harder to observe since the directivity curves will be dominated by propagating modes and the modes near cutoff will not provide a large contribution to the total sound field.

The p_M^+ mode amplitudes are, in principle, more appropriate for use in computing far field directivities because these are the modes used in the formulation of the radiation code. For cases containing well cut on modes, the use of p_M mode amplitudes will do an adequate job of estimating far field directivities with a significant saving of the computational effort involved in determining the p_M^+ mode amplitudes. For cases with relatively few modes propagating with one near cutoff, determination of the appropriate p_M^+ mode amplitude should be used.

One assumption has been made in the calibration procedure for obtaining the D_{MM} matrix elements: As presently written, the radiation code takes the coordinate system origin (x/r = 0) as common to both the inlet duct flow and the acoustic field. Thus, in calibrating with the sound source in the microphone plane, which is necessary, the axial flow in this plane is automatically constrained by the code procedure to be constant from hub to tip. This uniform distribution is an artifact of the code.

Overcoming this limitation would require revising the code so that the flow origin is taken at the fan face, and then imposing the calibrating acoustic modes at the microphone. Feasibility of making such a change in the radiation code might be investigated in the future, but whether the results would be sufficiently different from the present ones can not be predicted in advance.

Application 2

As described in the Analysis section, the objective of this application is to determine the modal output at the fan face, p_F^+, using the same microphone data, p_M, that has been presented. It should be mentioned that the numerical procedure followed to obtain the elements of D_{MF} differs in one significant aspect from that used in Application 1:

In Application 1 the source of the p^+ waves coincides with the radial plane containing the microphone pressures, p_M. This plane, shown in Figure 3, is the left–hand boundary of the finite element mesh, and there were 43 mesh points extending radially from the inner radius of the duct to outer radius, at which the radiation code computes the total pressure, p_M.

For Application 2, however, the mesh starts at the fan face, downstream from the microphone plane. Figure 6 shows the left boundary of the mesh being in a radial plane. But it is also seen that the microphone plane cuts through the mesh cells in a complicated way, due to the mesh curvature. Since pressures are required at points in the radial microphone plane, and the radiation code gives the pressures along cell boundaries, a 2–dimensional interpolation is needed. A substantial effort was involved in devising and applying a suitable procedure. For this procedure a second degree polynomial in variables x and r with complex coefficients was chosen to represent the pressure in the neighborhood of each point in the radial microphone plane for which the pressure must be interpolated:

$$p(x,r) = a_1 + a_2 x + a_3 x^2 + a_4 r + a_5 x\, r + a_6 r^2$$

Values of the 6 complex coefficients were obtained by fitting this function to the 6 points on the mesh closest to the interpolation point, (x,r). This required solving 6 simultaneous equations for each of the interpolation points.

Note: In the above descriptions, statements are made that pressures computed by the radiation code lie along the mesh lines. This was done to simplify the presentation for a casual reader. However, anyone intending to use the enhanced microphone system, should be aware that the pressures are really not calculated along mesh lines, but rather, at so–called "Gauss points", which happen to lie inside of each cell. The subject of Gauss points is handled in Reference 5)

Calibrations were then made to obtain D_{MF} elements for the same ADP conditions used in Application 1: Blade passage frequency at 9,600 rpm, 11,400 rpm, 12,000 rpm, and 2BPF at 9,600 rpm.

The fan–generated modes, p_F^+, were computed by Equation 13 from the measured microphone values, p_M. Table 1 lists p_M and p_F^+ for the first 4 radial modes of BPF at the 3 rig speeds.

The listed numbers are the decibel values, re. one Pascal, of the mode amplitudes, and the enormous differences between p_M and p_F^+ for the propagating modes are an indication of a serious problem with the analysis system. In Application 1, p_M and its component, p_M^+, were found to be quite simi-

lar, so for a propagating mode, the fan pressure p_F^+ should not be nearly as high as listed in Table 1. To verify this contention, calculations were made, using the radiation code, of the duct pressure, p, at a sequence of axial positions, x, upstream of the fan resulting from unit values of fan–generated modes, p_F^+.

Samples of these calculated results are plotted in Figures 13 and 14 for 9,600 rpm and 12,000 rpm, respectively. In both Figures 13 and 14 the designations a, b, c, and d indicate that the single unit fan forward mode applied to the system was the first, second, third, and fourth, successively. Increments of 0.05 units of x (normalized by duct radius) were taken between x/r = 0 and 0.8. (The microphone plane in the ADP rig tests was at x/r = 0.6.)

These figures clearly show that the levels of propagating modes vary only moderately from the origin at x/r = 0 to microphone location (x/r = 0.6). (Modes below cutoff are shown to decay exponentially, with higher modes decaying more rapidly.)

Consequently, the values of p_F^+ in Table 1 inferred from measured microphone data, p_M, are obviously wrong.

To clarify matters a sensitivity study was conducted that indicated the effect upon p_F^+ of microphone errors in the measured test data, p_M. Computer simulation using known inputs, p_F^+, to the finite element code was used to generate presumably accurate values of the total microphone pressure, p_M. These outputs were then perturbed by amounts ranging from 0.1 dB to 0.5 dB to simulate errors in p_M due to data acquisition and processing in an actual test. These perturbed values of p_M were then used in Equation 13 to obtain the source fan modes, p_F^+. Differences between these p_F^+ and the initially known p_F^+ values provided indications of the sensitivity of the process to microphone measurement error.

Details of these sensitivity studies are presented in Appendix B. While, in the rig tests, the microphone plane was located at a distance x/r of 0.6, the computer simulated runs were made for a series of hypothetical microphone locations of x/r = 0 to 0.8 in steps of 0.05 to reveal detailed behavior of the system as the microphone plane successively moved farther along the axis from the fan.

The fan–to–microphone separation turned out to be a critical parameter. For separations of less than x/r ≈ 0.2, good results were obtained using the first 4 radial modes, and these improved as x/r approached zero. (This characteristic showed that the procedures involved in Application 1 were reliable since the source–to–microphone distance used in computer calibrations was essentially zero there.)

For distances greater than x/r = 0.2 results progressively degenerated; the computed values of p_F^+ differed more and more from the known input values. For the actual test microphone location at x/r = 0.6, the computed values of p_F^+ had no recognizable relation to the initial known fan mode inputs.

On the basis of a conjecture that low levels of decaying modes at large microphone distances were responsible for the problem, the procedure was repeated with an important modification: Instead of using 4 radial modes to fit microphone point data it was decided to resolve the point data into only the propagating modes (or, into those plus a weakly decaying mode, if present.)

This modification worked. The perturbed microphone data gave back the known inputs satisfactorily for x/r = 0.6 and beyond, as seen in Appendix B.

On the basis of the sensitivity studies, it is possible to select a least squares fit to give reasonable results for fan noise prediction, p_F^+, from the actual microphone test data, where x/r = 0.6. For blade–passage frequency at the 3 speeds 9,600, 11,400, and 12,000 a least squares fit of the microphone data to 2 modes was used. The harmonic, 2BPF, at 9,600, having 3 propagating modes could be resolved into these 3 modes.

Table 2 gives the inputs, p_M, and the fan source mode structure, p_F^+, for the selected rig speeds. At 9600 rpm, the BPF mode μ=1 is cut off. For this reason there is a larger difference between p_M and p_F^+ for this case than for the remaining modes which are all cut on. The fan face level, p_F^+, is also higher than the level at the microphone, p_M. Well cuton modes show smaller differences between p_F^+ and p_M with the p_M levels larger. This results from the variation of geometry and flow velocity throughout the inlet. Figures 13 and 14 show examples of mode amplitude variations within the duct. Modes just above cutoff, such as BPF mode μ=1 at 11,400 rpm and 2BPF mode μ=2 at 9,600 rpm, result in larger differences between p_F^+ and p_M than well cut on modes.

If, in future programs, it is deemed essential to obtain information about decaying modes generated by the fan, further sensitivity studies must be made. For example, it may turn out that a different inlet configuration, providing a closer fan–to–microphone spacing (lower value of x/r) will work. The so–called "short inlet" should give a value of x/r of about 0.25. Computer simulation studies could be made to determine if reliable results can be extended to 4 modes.

CONCLUSIONS AND RECOMMENDATIONS

In using measurements from rotating microphones in fan inlets to predict far field directivity patterns, waves reflected from the inlet mouth back to the microphones can lead to significant errors in the predictions. A procedure has been derived for minimizing these effects by use of a finite element radiation code that separates upstream–going waves from downstream–going waves.

Via an analytical simulation, it was shown, for a mode near cutoff, that far field projections could vary erroneously by large amounts, depending on where the rotating microphone plane happened to be in the internal standing wave pattern. The enhanced data reduction scheme successfully collapsed the error band to about 0.5 dB. The system was then applied to four test runs of the 17 inch ADP fan model where the rotating mic data were available. Comparison of far field projections using the basic and enhanced schemes yielded nearly the same results, apparently because the mic array was not near a node in the standing wave pattern. For conditions that include modes near cutoff and mic array locations near standing wave nodes, the enhanced scheme can make a significant improvement in accuracy of far field projections. A criterion is needed for when the enhanced scheme is needed (based, say on cutoff ratio).

It is also recommended that a modification to the radiation code be examined for feasibility: The present code uses a common plane as the source of both the noise and flow and the same grid for each field. Studies such as those discussed in this report require that the location of the noise source be taken at various axial locations within the duct. The result is that the details of the flow field change slightly as the location of the noise input is changed. To eliminate this, means should be found to allow separate input planes for the noise and flow, possibly by interpolating the flow field onto the desired noise grid.

For the Application 2 task, which consists of determining the fan mode structure, p_F^+, from microphone measurements, p_M, using measured data where the normalized fan to microphone distance, x/r, was 0.6, it is concluded that only propagating or weakly decaying modes be employed.

If in other configurations, the fan and microphone planes are closer together ($x/r \leq 0.2$) it is concluded that decaying modes can also be found.

It is recommended that, in planning other tests and fan configurations, sensitivity studies be made at an early stage to determine what features are needed to allow recovery of the desired information.

A correlary recommendation, applicable to existing test data on the 17" ADP rig, is to analyze the so–called short inlet configuration to see if the closer fan–to–microphone spacing will allow recovery of the decaying modes.

APPENDIX A
NOTATION

a,b,c,d	constants
$a_1 \ldots a_6$	coefficients of interpolation polynomial
BPF	fan blade passage frequency (Hz.)
C_{mu}	coefficient of (m,μ) circumferential–radial mode
D, D^{-1}	calibration matrix, inverse
D_{MF}, D_{MF}^{-1}	calibration matrix relating p at mic plane to p^+ at fan face
D_{MM}, D_{MM}^{-1}	calibration matrix relating p at mic plane to p^+ at mic plane
expi(z)	complex exponential function, e^{iz}
I	unit matrix
J_m	Bessel function of the first kind of order m
$k_{m\mu}$	eigenvalue for (m,μ) mode
m	circumferential mode index
p	total acoustic pressure, $p^+ + p^-$
p^+	upstream traveling acoustic pressure component
p^-	downstream traveling acoustic pressure component
p_F^+	upstream traveling acoustic pressure component at fan face
p_M	total acoustic pressure at mic plane
p_M^+	upstream traveling acoustic pressure component at mic plane
p_M^-	downstream traveling acoustic pressure component at mic plane
P	complex acoustic pressure
p_1, p_2, p_3	mode components sum of upstream and downstream components
p_1^+, p_2^+, p_3^+	upstream traveling mode components
p_1^-, p_2^-, p_3^-	downstream traveling mode components
p_μ	mode amplitude coefficient = C_{mu}
$Q_{m\mu}$	eigenvalue for (m,μ) mode
r	radial coordinate
t	time
T	vector transpose (superscript)
x	axial coordinate
Y_m	Bessel function of the second kind of order m
θ	circumferential coordinate
μ	radial mode index (0,1, ...)
$\Psi_{m\mu}(r)$	mode radial shape function
ω	radian frequency = 2π x frequency

APPENDIX B
SENSITIVITY STUDIES

The general basis for these studies is to use computer simulation with postulated, <u>known</u> fan modes p_F^+ as inputs to the radiation code in order to obtain the outputs, p_M. These outputs were perturbed by small amounts and the perturbed quantities were inserted into Equation 13 to simulate the problem of obtaining p_F^+ from p_M. The resulting p_F^+ values and their deviations from the known input provided a guide to the effects of small variations in the "data". Rather than using just the test microphone location at $x/r = 0.6$, the process was applied over the range of mic. locations between $x/r = 0$ to $x/r = 0.8$ in steps of 0.05 to find how the results varied with source–to–microphone separation.

At each rig speed one of a sequence of unit p_F^+ modes, $[1,0,0,0]^T$, $[0,1,0,0]^T$, etc. was applied. Values of p_M were obtained from the radiation code, and were perturbed according to the following scheme:

It was assumed that microphone reading errors could be expressed as a fraction of 1 decibel and these were applied to the modal coefficients, p_M, as follows.

If $|p_M| = \begin{bmatrix} a \\ b \\ c \\ d \end{bmatrix}$ (Pascals) and the perturbations were arbitrarily taken as $\begin{bmatrix} 0.5 \\ -0.4 \\ 0.3 \\ 0.1 \end{bmatrix}$ dB ,

then the values of p_M would be replaced by multiplying them by factors of $10^{dB/20}$, giving the perturbed vector

$$\begin{bmatrix} 10^{.5/20} \ a \\ 10^{-.4/20} \ b \\ 10^{.3/20} \ c \\ 10^{.1/20} \ d \end{bmatrix} = \begin{bmatrix} 1.059 \ a \\ 0.955 \ b \\ 1.035 \ c \\ 1.012 \ d \end{bmatrix} \quad \text{(Pascals)}$$

(Note a,b,c,d are the amplitudes of the complex quantities; the phase angles were left unchanged.)

Table 3A gives the results of the process for BPF at 12,000 rpm. The fan mode exciting the system is a unit magnitude $\mu = 0$ mode, $[1,0,0,0]^T$. If the resulting values of p_M were <u>not</u> perturbed, the computed values of p_F^+ would be exactly equal to the input, $[1,0,0,0]$ Pascals. In decibel units, the tabulated values in the successive colums would be 0 dB, $-\infty$ dB, $-\infty$ dB, and $-\infty$ dB, and these would hold for all distances x/r from 0 to 0.8.

With the perturbed values of p_M, examination of the first 2 or 3 lines, where the microphone and fan face are close together reveals two features: The first column values, corresponding to the $\mu = 0$ unit input mode are very close to the assumed perturbation of 0.5 dB. The last 3 column values are at least 40 dB down, which is very good from a practical viewpoint.

Switching attention now to Table 3B, which gives results for unit $\mu = 1$ mode, $[0,1,0,0]^T$, the second column values are close to the perturbation of -0.4 dB: all other columns are way down for x/r small. Corresponding results are obtained for unit $\mu = 2$ and 3 inputs, as shown in Tables 3C and 3D.

In summary, for sufficiently small x/r, the process of obtaining the fan mode structure p_F^+ from microphone readings, p_M subject to small error, is very well–behaved; errors in the result are proportionate to errors in the measured values p_M.

However, as x/r increases, the nature of the results changes markedly – calculated values of all modes grow, until at the upper limit, x/r = 0.8, the listed pressures of all modes are manifestly absurd. This progressive degeneration holds for all 4 excitations, shown in Figures 3A thru 3D. For the microphone location x/r = 0.6 where actual rig data were acquired, examination of the set of Figures 2 shows obviously unacceptable results.

Similar results were obtained for BPF at 9,600 rpm and 11,400 rpm, and for 2BPF at 9,600 rpm. In addition, the entire set of calculations was repeated using different perturbations: 0.3dB, 0.1dB, 0.5dB and –0.4dB. These showed the same trends as just described; good results for small x/r, degrading to very poor information at the test microphone location, x/r = 0.6.

It is clear that any future testing of fan configurations should be preceded by computer–simulated runs using the appropriate parameters in the radiation code. By this means, the test microphone location can be selected in advance to give reliable predictions of the fan source strength, p_F^+.

In an attempt to find some useful information about source excitation, p_F^+, from the ADP rig data on hand, it was conjectured that if resolution of the microphone data by least squares fit to 4 modes were to be fit instead to fewer, lower order modes, the results might be a valid measure of the propagating modes present. It may be that decaying modes at x/r = 0.6 are sufficiently contaminated by system "noise" so as to give a false prediction of the source, and that by simply eliminating them from the model, the remaining modes could be found reliably. Fortunately, this turned out to be true, as shown in Tables 4,5,6, and 7.

Table 4 applies to BPF at 9,600 rpm. Only the $\mu = 0$ mode propagates, but the $\mu = 1$ mode does not decay very rapidly and was included in a least squares fit. The perturbations were 0.5 dB and –0.4 dB, as before. (Modes $\mu = 2$ and $\mu = 3$ and their perturbations are simply absent throughout the process. Table 4A gives results vs. x/r for unit $\mu = 0$ input, and Table 4B is for unit $\mu = 1$ mode. Results are clearly satisfactory at x/r = 0.6 (The results initially obtained for a 4–mode fit at this speed were useless at x/r = 0.6; for brevity they are not shown in this report.)

Tables 5A and 5B are for 11,400 rpm, where the first two modes propagate.

Tables 6A and 6B represent results at 12,000 rpm, where there are still 2 propagating modes. Again results at x/r = 0.6 are satisfactory.

Tables 7A, B, C apply to twice blade passage frequency at 9,600 rpm. Here, the first 3 modes are propagating and a corresponding 3–mode least squares fit was used for p_M. Three tables, A, B, C, are now needed to display the result of perturbations 0.5, –0.4, and 0.3. It is evident that results are good, not only at x/r = 0, but all the way to 0.8.

These sensitivity studies also reveal information about Application 1 type tests. These tests involve extracting the forward component, p_M^+ at the microphone plane, rather than at the fan, p_F^+, from total microphone pressure, p_M. The sensitivity studies show that when the plane, p_M is close to the p^+ plane the prediction scheme using all 4 modes works well. In Application 1, these planes are coincident (x/r $\approx$ 0) so that the results obtained there can be regarded with confidence.

REFERENCES

1. Cicon, D. E., Sofrin, T. G., and Mathews, D. C., "Investigation of Continuously Traversing Microphone System for Mode Measurement", NASA CR–168040, November, 1982.

2. Heidelberg, L. J., and Hall, D. G., "Acoustic Mode Measurements in the Inlet of a Model Turbofan Using a Continuously Rotating Rake", AIAA Paper No. 93–0589, January, 1993.

3. Hall, D. G., Heidelberg, L., and Konno, K., "Acoustic Mode Measurements in the Inlet of a Model Turbofan Using a Continuously Rotating Rake: Data Collection/Analysis Techniques", AIAA Paper No. 93–0599, January, 1993.

4. Woodward, R. P., Bock, L. A., Heidelberg, L. J., and Hall, D. G., "Far–Field Noise and Internal Modes From a Ducted Propeller at Simulated Aircraft Takeoff Conditions", AIAA Paper No. 92–0371, January, 1992.

5. Roy, I.D., Eversman, W., and Meyer, H.D., "Improved Finite Element Modeling of the Turbofan Engine Inlet Radiation Problem," NASA Contractor Report for NAS3–25952, Task 10, April, 1993.

6. Moore, C. J., "Measurement of Radial and Circumferential Modes in Annular and Circular Fan Ducts", Journal of Sound and Vibration, Vol. 62, No. 2, pp. 235–256, 1979.

TABLE 1

Fan–generated Mode Amplitudes, p_F^+, Computed from Measured Microphone Values, p_M, Using Equation 13. All Amplitudes have Units of Decibels re. One Pascal.

Blade Passage Frequency

Mode No.	9,600 rpm		11,400 rpm		12,000 rpm	
	p_M	p_F^+	p_M	p_F^+	p_M	p_F^+
0	33.5	62.2	31.6	62.1	28.4	69.1
1	24.4	63.3	27.8	66.5	27.0	73.2
2	16.6	79.3	13.6	76.7	35.8	84.5
3	17.6	99.4	20.8	98.2	31.2	104.8

TABLE 2

Fan Modes, p_F^+, from variable Least Squares fit of Microphone Modes, p_M
All Amplitudes have Units of Decibels re. One Pascal.

Mode No. μ.	BPF 9,600 rpm		BPF 11,400 rpm		BPF 12,000 rpm		2BPF 9,600 rpm	
	p_M	p_F^+	p_M	p_F^+	p_M	p_F^+	p_M	p_F^+
0	33.5	30.4	31.7	28.1	27.9	24.1	47.1	47.2
1	24.0	41.2	27.2	22.5	25.9	24.9	45.0	42.7
2							48.3	40.3

TABLE 3A

Fan–generated Mode Amplitudes, p_F^+, Computed from Perturbed Microphone Values, p_M, Using Equation 13. All Amplitudes have Units of Decibels re. One Pascal.

Blade Passage Frequency

12,000 rpm

Input mode, $p_F^+ = [1,0,0,0]^T$

Distance x/r	Mode $\mu=0$	Mode $\mu=1$	Mode $\mu=2$	Mode $\mu=3$
0.00	0.4983	–42.0939	–60.6872	–63.9803
0.05	0.4968	–42.1069	–51.3050	–51.5325
0.10	0.4993	–44.0812	–45.1004	–42.5006
0.15	0.4968	–52.6600	–42.4603	–34.7413
0.20	0.4862	–39.9090	–53.1564	–26.5955
0.25	0.4620	–33.5101	–35.5056	–19.5173
0.30	0.4428	–32.0718	–27.3077	–11.2002
0.35	0.4755	–33.1389	–22.6374	–2.5900
0.40	0.6716	–27.6733	–15.4206	6.1875
0.45	1.1256	–18.7334	–7.2096	14.2228
0.50	1.4583	–12.7149	–0.6964	20.3841
0.55	2.7357	–3.0345	8.5145	28.9615
0.60	0.3406	–0.2393	11.4179	31.2333
0.65	11.8982	14.2791	26.1699	46.0359
0.70	21.2753	24.4680	36.3513	56.2520
0.75	28.7842	32.5388	44.4155	64.3228
0.80	39.5239	43.5666	55.4345	75.3530

($\mu=0$, $\mu=1$ propagating)

TABLE 3B

Fan–generated Mode Amplitudes, p_F^+, Computed from Perturbed Microphone Values, p_M, Using Equation 13. All Amplitudes have Units of Decibels re. One Pascal.

Blade Passage Frequency

12,000 rpm

Input mode, $p_F^+ = [0,1,0,0]^T$

Distance x/r	Mode μ=0	Mode μ=1	Mode μ=2	Mode μ=3
0.00	–60.7032	–0.4001	–42.3374	–56.9170
0.05	–47.6168	–0.3984	–36.9705	–46.7569
0.10	–42.7402	–0.3986	–32.0085	–37.5835
0.15	–42.6137	–0.3851	–27.1599	–29.2593
0.20	–42.6407	–0.3419	–21.8361	–21.0339
0.25	–40.5633	–0.2695	–17.4699	–13.4298
0.30	–37.3929	–0.2245	–13.7425	–5.6653
0.35	–29.7582	–0.3975	–10.1966	1.6835
0.40	–24.1306	–0.9456	–6.5995	9.1528
0.45	–18.2286	–1.7903	–1.3621	16.9708
0.50	–11.5820	–0.3011	5.5007	24.4950
0.55	6.7835	10.0674	22.0657	42.6680
0.60	6.9592	12.8882	23.2836	42.8051
0.65	15.6758	20.5211	31.8811	51.4782
0.70	23.8776	28.2255	39.9511	59.6682
0.75	32.2267	36.3542	48.1713	68.0105
0.80	43.1881	47.2124	59.0526	78.9717

(μ=0, μ=1 propagating)

TABLE 3C

Fan–generated Mode Amplitudes, p_F^+, Computed from Perturbed Microphone Values, p_M, Using Equation 13. All Amplitudes have Units of Decibels re. One Pascal.

Blade Passage Frequency

12,000 rpm

Input mode, $p_F^+ = [0,0,1,0]^T$

Distance x/r	Mode μ=0	Mode μ=1	Mode μ=2	Mode μ=3
0.00	−71.9642	−60.2117	0.2996	−64.7547
0.05	−70.3679	−57.6402	0.2998	−59.2213
0.10	−68.8556	−54.2661	0.2986	−52.7881
0.15	−68.6473	−49.9164	0.2933	−46.2554
0.20	−65.3853	−46.1812	0.2767	−40.4471
0.25	−61.1792	−45.3530	0.2431	−36.6649
0.30	−61.8010	−46.3129	0.2044	−33.8795
0.35	−60.2849	−46.1968	0.2028	−26.1994
0.40	−52.8500	−44.4384	0.3137	−15.8930
0.45	−42.9073	−38.5787	0.5832	−6.3098
0.50	−34.2576	−30.5533	0.8524	1.9737
0.55	−17.4971	−13.6060	4.8727	18.3904
0.60	−16.2695	−12.3818	2.3403	19.5278
0.65	−7.3879	−3.4279	7.6714	28.3869
0.70	1.3164	5.3137	16.4532	37.0983
0.75	9.6988	13.7048	25.1665	45.4828
0.80	20.2520	24.2569	35.9951	56.0359

(μ=0, μ=1 propagating)

TABLE 3D

Fan–generated Mode Amplitudes, p_F^+, Computed from Perturbed Microphone Values, p_M, Using Equation 13. All Amplitudes have Units of Decibels re. One Pascal.

Blade Passage Frequency

12,000 rpm

Input mode, $p_F^+ = [0,0,0,1]^T$

Distance x/r	Mode μ=0	Mode μ=1	Mode μ=2	Mode μ=3
0.00	−66.6672	−66.3373	−57.5148	0.1036
0.05	−74.0001	−61.4967	−56.1559	0.1032
0.10	−68.0009	−59.8443	−54.0236	0.1021
0.15	−65.1911	−59.4957	−51.6988	0.0973
0.20	−64.5384	−59.1168	−48.9465	0.0846
0.25	−65.2605	−59.2930	−46.0591	0.0749
0.30	−67.5697	−59.5946	−43.8164	0.0920
0.35	−69.9456	−56.9243	−42.6455	0.2276
0.40	−71.8641	−53.6292	−42.6046	0.4047
0.45	−59.9777	−50.3142	−40.4912	0.3966
0.50	−49.2954	−44.9420	−31.7806	−0.6079
0.55	−25.8315	−21.8919	−10.4258	10.6707
0.60	−26.0609	−22.1812	−9.6313	6.7499
0.65	−15.6523	−11.6949	0.5281	19.1797
0.70	−6.1688	−2.1730	9.8458	29.3193
0.75	2.2951	6.3003	18.2210	37.9985
0.80	12.5441	16.5493	28.4219	48.3259

(μ=0, μ=1 propagating)

TABLE 4A

Fan–generated Mode Amplitudes, p_F^+, Computed from Perturbed Microphone Values, p_M, Using Equation 13. All Amplitudes have Units of Decibels re. One Pascal.

Blade Passage Frequency

9,600 rpm

Input mode, $p_F^+ = [1,0]^T$

Distance x/r	Mode $\mu=0$	Mode $\mu=1$
0.00	0.4979	−39.5877
0.05	0.4975	−36.7478
0.10	0.4962	−34.1682
0.15	0.4935	−31.7672
0.20	0.4874	−29.3507
0.25	0.4780	−27.2583
0.30	0.4682	−25.5668
0.35	0.4630	−24.7413
0.40	0.4649	−24.3966
0.45	0.4772	−24.5669
0.50	0.5000	−24.5604
0.55	0.5484	−21.3420
0.60	0.5361	−20.2751
0.65	0.5051	−18.2635
0.70	0.4331	−15.2950
0.75	0.3703	−7.6076
0.80	0.5021	1.3457

($\mu=0$ propagating)

TABLE 4B

Fan–generated Mode Amplitudes, p_F^+, Computed from Perturbed Microphone Values, p_M, Using Equation 13. All Amplitudes have Units of Decibels re. One Pascal.

Blade Passage Frequency

9,600 rpm

Input mode, $p_F^+ = [0,1]^T$

Distance x/r	Mode μ=0	Mode μ=1
0.00	–51.9017	–0.3989
0.05	–50.3314	–0.3984
0.10	–49.6326	–0.3970
0.15	–49.1280	–0.3940
0.20	–47.0167	–0.3873
0.25	–44.3997	–0.3768
0.30	–43.0632	–0.3661
0.35	–42.7220	–0.3604
0.40	–43.1054	–0.3625
0.45	–43.6889	–0.3760
0.50	–44.2512	–0.4011
0.55	–40.8661	–0.4552
0.60	–44.7555	–0.4414
0.65	–45.3858	–0.4066
0.70	–46.2091	–0.3275
0.75	–46.8506	–0.2578
0.80	–44.4952	–0.3723

(μ=0 propagating)

TABLE 5A

Fan–generated Mode Amplitudes, p_F^+, Computed from Perturbed Microphone Values, p_M, Using Equation 13. All Amplitudes have Units of Decibels re. One Pascal.

Blade Passage Frequency

11,400 rpm

Input mode, $p_F^+ = [1,0]^T$

Distance x/r	Mode $\mu=0$	Mode $\mu=1$
0.00	0.4958	−36.3481
0.05	0.4951	−38.1990
0.10	0.4937	−38.0061
0.15	0.4888	−37.0658
0.20	0.4827	−35.8805
0.25	0.4802	−35.3279
0.30	0.4789	−35.9649
0.35	0.4647	−31.9297
0.40	0.4391	−28.3415
0.45	0.4336	−28.5792
0.50	0.4506	−30.3333
0.55	0.4846	−34.0732
0.60	0.4931	−44.9382
0.65	0.4943	−40.1698
0.70	0.4860	−33.6664
0.75	0.4708	−31.4760
0.80	0.4384	−30.9866

($\mu=0$, $\mu=1$ propagating)

TABLE 5B

Fan–generated Mode Amplitudes, p_F^+, Computed from Perturbed Microphone Values, p_M, Using Equation 13. All Amplitudes have Units of Decibels re. One Pascal.

Blade Passage Frequency

11,400 rpm

Input mode, $p_F^+ = [0,1]^T$

Distance x/r	Mode μ=0	Mode μ=1
0.00	–51.9393	–0.3965
0.05	–50.8032	–0.3959
0.10	–47.4501	–0.3943
0.15	–41.7832	–0.3889
0.20	–37.7854	–0.3821
0.25	–35.9670	–0.3794
0.30	–35.8325	–0.3778
0.35	–35.5587	–0.3623
0.40	–34.6581	–0.3342
0.45	–33.8977	–0.3282
0.50	–34.6274	–0.3468
0.55	–28.7592	–0.3837
0.60	–38.3118	–0.3936
0.65	–36.1119	–0.3949
0.70	–33.1425	–0.3855
0.75	–31.7557	–0.3686
0.80	–30.8946	–0.3333

(μ=0, μ=1 propagating)

TABLE 6A

Fan–generated Mode Amplitudes, p_F^+, Computed from Perturbed Microphone Values, p_M, Using Equation 13. All Values have Units of Decibels re. One Pascal.

Blade Passage Frequency

12,000 rpm

Input mode, $p_F^+ = [1,0]^T$

Distance x/r	Mode $\mu=0$	Mode $\mu=1$
0.00	0.4983	-41.5396
0.05	0.4969	-41.3311
0.10	0.5001	-43.2448
0.15	0.4991	-54.1553
0.20	0.4914	-40.6982
0.25	0.4733	-33.7336
0.30	0.4560	-31.3059
0.35	0.4559	-31.6531
0.40	0.4618	-33.0684
0.45	0.4628	-32.1487
0.50	0.4552	-28.9901
0.55	0.5056	-28.1050
0.60	0.4890	-34.2181
0.65	0.4989	-47.0594
0.70	0.4806	-33.4832
0.75	0.4516	-29.8826
0.80	0.4061	-29.0436

($\mu=0$, $\mu=1$ propagating)

TABLE 6B

Fan–generated Mode Amplitudes, p_F^+, Computed from Perturbed Microphone Values, p_M, Using Equation 13. All Values have Units of Decibels re. One Pascal.

Blade Passage Frequency

12,000 rpm

Input mode, $p_F^+ = [0,1]^T$

Distance x/r	Mode μ=0	Mode μ=1
0.00	–60.3535	–0.3993
0.05	–47.7771	–0.3978
0.10	–42.4365	–0.4014
0.15	–41.4934	–0.4003
0.20	–40.3622	–0.3917
0.25	–36.6253	–0.3717
0.30	–34.2635	–0.3526
0.35	–33.3539	–0.3525
0.40	–33.8858	–0.3590
0.45	–34.3899	–0.3601
0.50	–34.6144	–0.3516
0.55	–32.5263	–0.4067
0.60	–41.6366	–0.3891
0.65	–43.9171	–0.4000
0.70	–34.7168	–0.3797
0.75	–31.0264	–0.3474
0.80	–29.1392	–0.2978

(μ=0, μ=1 propagating)

TABLE 7A

Fan–generated Mode Amplitudes, p_F^+, Computed from Perturbed Microphone Values, p_M, Using Equation 13. All Amplitudes have Units of Decibels re. One Pascal.

Twice Blade Passage Frequency

9,600 rpm

Input mode, $p_F^+ = [1,0,0]^T$

Distance x/r	Mode μ=0	Mode μ=1	Mode μ=2
0.00	0.4981	−57.6101	−60.5270
0.05	0.4972	−54.2157	−60.7388
0.10	0.4963	−50.0314	−69.3182
0.15	0.4931	−43.0440	−56.8064
0.20	0.4842	−39.2625	−50.6235
0.25	0.4782	−37.9375	−55.2916
0.30	0.4701	−35.7663	−51.9492
0.35	0.4541	−33.6034	−42.3256
0.40	0.4453	−33.0857	−40.4393
0.45	0.4419	−32.4335	−42.4967
0.50	0.4395	−31.5047	−41.2395
0.55	0.4504	−32.2531	−40.7099
0.60	0.4755	−34.7792	−43.6341
0.65	0.4932	−38.6193	−49.2649
0.70	0.4941	−66.9818	−48.2364
0.75	0.4566	−35.4951	−38.1099
0.80	0.3720	−30.7390	−33.2868

(μ=0, μ=1, μ=2 propagating)

TABLE 7B

Fan–generated Mode Amplitudes, p_F^+, Computed from Perturbed Microphone Values, p_M, Using Equation 13. All Amplitudes have Units of Decibels re. One Pascal.

Twice Blade Passage Frequency

9,600 rpm

Input mode, $p_F^+ = [0,1,0]^T$

Distance x/r	Mode μ=0	Mode μ=1	Mode μ=2
0.00	−59.7327	−0.3981	−44.6300
0.05	−48.4808	−0.3966	−42.4633
0.10	−44.2941	−0.3922	−38.2509
0.15	−42.0531	−0.3777	−36.7339
0.20	−37.1942	−0.3689	−37.7396
0.25	−35.2459	−0.3510	−35.1722
0.30	−34.4992	−0.3116	−31.2076
0.35	−33.2442	−0.2498	−29.7316
0.40	−32.7316	−0.2221	−28.9187
0.45	−32.6315	−0.2310	−29.0618
0.50	−32.5768	−0.2427	−30.0752
0.55	−33.3115	−0.2681	−31.2239
0.60	−36.0627	−0.3199	−32.5301
0.65	−39.3813	−0.3613	−33.5881
0.70	−39.6106	−0.3492	−32.2830
0.75	−33.5685	−0.2667	−30.7972
0.80	−29.8096	−0.1215	−30.2460

(μ=0, μ=1, μ=2 propagating)

TABLE 7C

Fan–generated Mode Amplitudes, p_F^+, Computed from Perturbed Microphone Values, p_M, Using Equation 13. All Amplitudes have Units of Decibels re. One Pascal.

Twice Blade Passage Frequency
9,600 rpm

Input mode, $p_F^+ = [0,0,1]^T$

Distance x/r	Mode μ=0	Mode μ=1	Mode μ=2
0.00	−72.6975	−50.7547	0.2979
0.05	−63.0772	−53.0153	0.2975
0.10	−60.5412	−48.2286	0.2942
0.15	−64.4835	−39.8584	0.2840
0.20	−64.4049	−36.9821	0.2850
0.25	−58.2798	−36.7788	0.2746
0.30	−50.5067	−35.3777	0.2461
0.35	−46.2464	−32.8241	0.2042
0.40	−45.6158	−32.3553	0.1869
0.45	−45.2430	−32.9497	0.1990
0.50	−44.8579	−33.3355	0.2125
0.55	−46.6272	−33.3128	0.2253
0.60	−53.3277	−34.7917	0.2483
0.65	−67.2021	−37.4127	0.2687
0.70	−47.1183	−35.4580	0.2566
0.75	−39.1491	−32.6590	0.2176
0.80	−34.2684	−31.8111	0.1657

(μ=0, μ=1, μ=2 propagating)
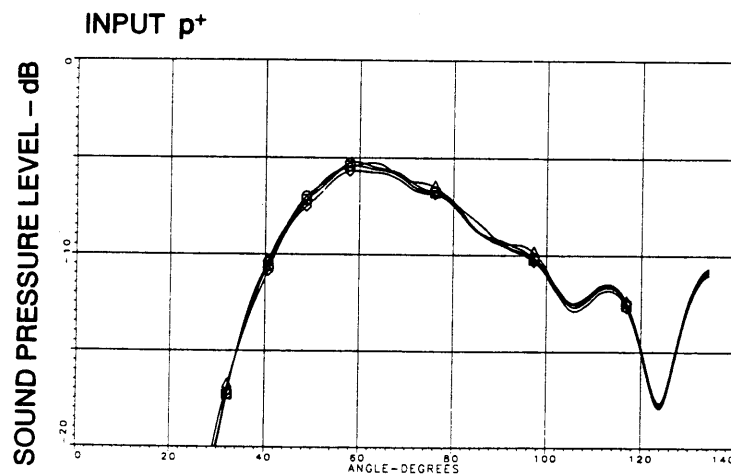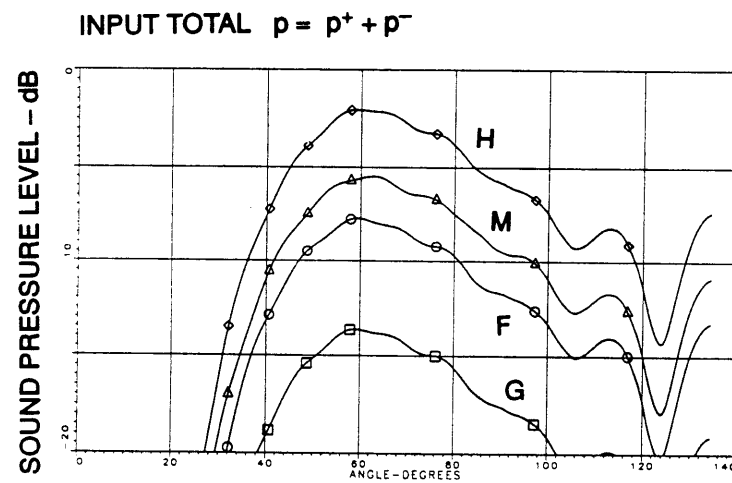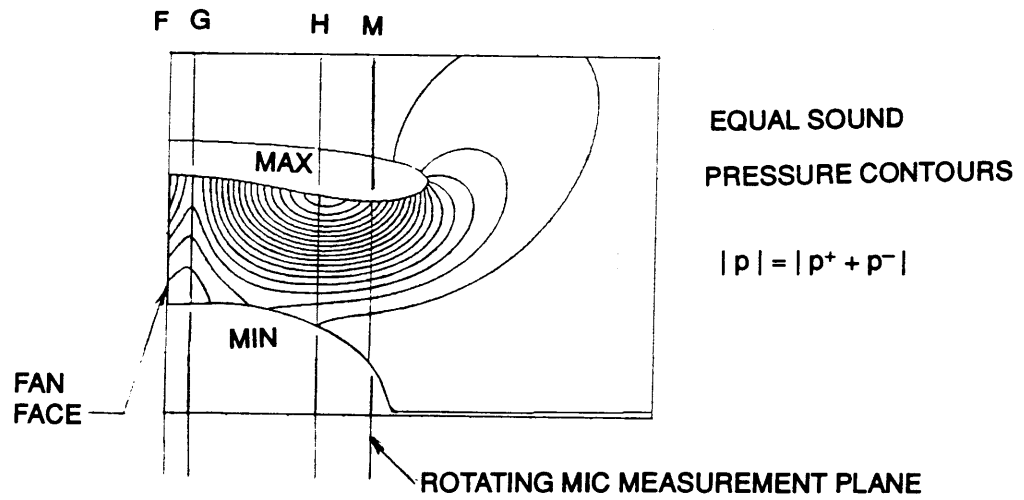
Figure 1.   Comparison of far field directivities for p and p $^+$ inputs at four axial locations. BPF at 7500 rpm. Mode = 6,0. Noise field obtained from unit input amplitude at the fan face.

$$\mathbf{p_M} = \mathbf{p_M^+} + \mathbf{p_{\bar{M}}}$$

Measured → ↑ ↖ Backward Wave Component

Required Forward Wave Component
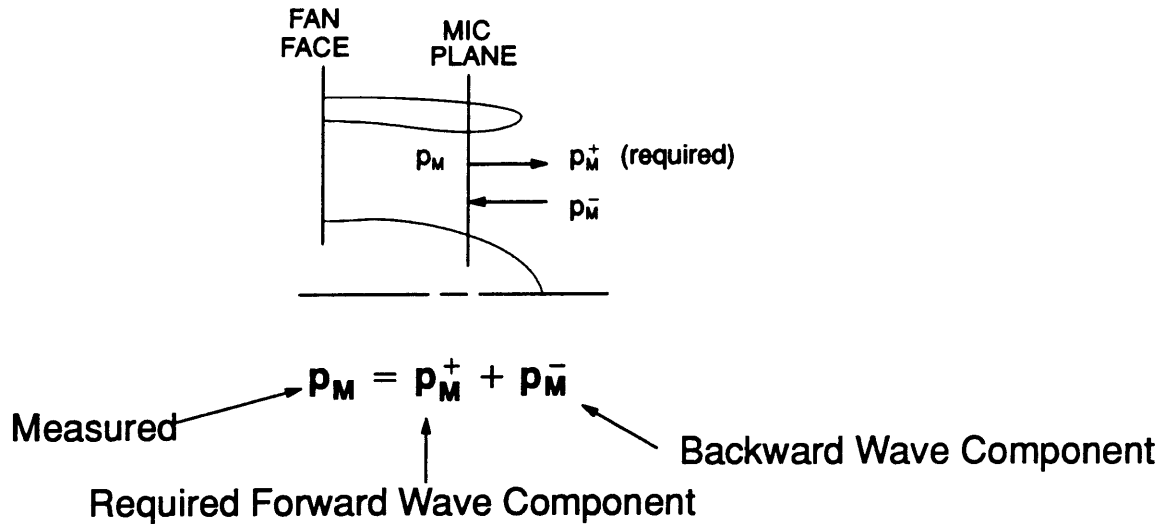
Relation $p_M = D_{MM}p_M{}^+$ determined by "calibration" with inlet radiation code.

In expanded form (for 3 radial modes):

Complex radial mode vector

$$\begin{bmatrix} p_1 \\ p_2 \\ p_3 \end{bmatrix}_M = \begin{bmatrix} D_{11} & D_{12} & D_{13} \\ D_{21} & D_{22} & D_{23} \\ D_{31} & D_{32} & D_{33} \end{bmatrix}_{MM} \bullet \begin{bmatrix} p_1{}^+ \\ p_2{}^+ \\ p_3{}^+ \end{bmatrix}_M$$

When elements of D_{MM} are known, any measured p_M can be resolved,

$$p_M{}^+ = D_{MM}{}^{-1}\, p_M$$

Figure 2. Application 1 – Method of obtaining forward waves, p_M^+, at the mic array from measured total pressures, p_M, at the same plane.
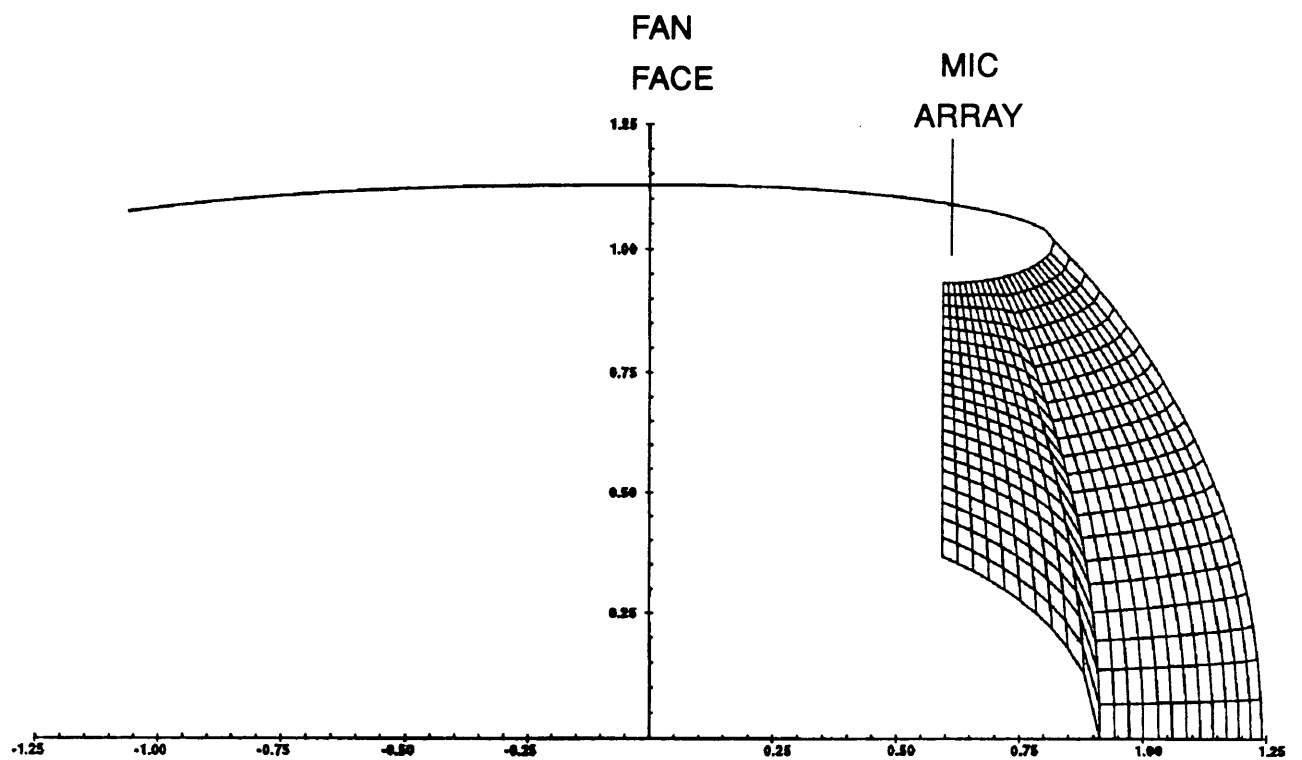
Figure 3.   Mesh system used to obtain forward waves, p_M^+, at the mic array from measured total pressures, p_M, at the same plane.

$$p_M = D_{MM}\, p_M^+$$

write as $\quad p = D\, p^+$

for 3x3
$$\begin{bmatrix} p_1 \\ p_2 \\ p_3 \end{bmatrix} = \begin{bmatrix} D_{11} & D_{12} & D_{13} \\ D_{21} & D_{22} & D_{23} \\ D_{31} & D_{32} & D_{33} \end{bmatrix} \begin{bmatrix} p_1^+ \\ p_2^+ \\ p_3^+ \end{bmatrix}$$

Calibrate with successive known, unit modal inputs

first $\begin{bmatrix} D_{11} \\ D_{21} \\ D_{31} \end{bmatrix} = \begin{bmatrix} & & \\ & & \\ & & \end{bmatrix} \begin{bmatrix} 1 \\ 0 \\ 0 \end{bmatrix}$ First unit input gives first column elements of D

second $\begin{bmatrix} D_{12} \\ D_{22} \\ D_{32} \end{bmatrix} = \begin{bmatrix} & & \\ & & \\ & & \end{bmatrix} \begin{bmatrix} 0 \\ 1 \\ 0 \end{bmatrix}$ Second unit input gives second column of D

third $\begin{bmatrix} D_{13} \\ D_{23} \\ D_{33} \end{bmatrix} = \begin{bmatrix} & & \\ & & \\ & & \end{bmatrix} \begin{bmatrix} 0 \\ 0 \\ 1 \end{bmatrix}$ Third unit input gives third column of D

Outputs from computer program are columns of D_{MM} matrix

Figure 4.   Computer calibrations to give elements of D_{MM}.
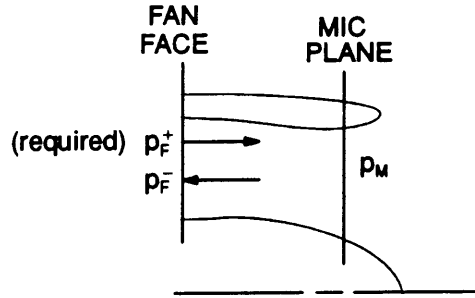
Relation $\qquad p_M = D_{MF}\, p_F^+$

In expanded form (for 3 radial modes):

Complex radial mode vector

$$\begin{bmatrix} p_1 \\ p_2 \\ p_3 \end{bmatrix}_M = \begin{bmatrix} D_{11} & D_{12} & D_{13} \\ D_{21} & D_{22} & D_{23} \\ D_{31} & D_{32} & D_{33} \end{bmatrix}_{MF} \bullet \begin{bmatrix} p_1{}^+ \\ p_2{}^+ \\ p_3{}^+ \end{bmatrix}_F$$

When elements of D_{MM} are known, any measured p_M can be resolved,

$$p_M{}^+ = D_{MF}{}^{-1}\, p_M$$

Figure 5.   Application 2 – Method of obtaining forward waves, p_F^+, at the fan face from measured total pressures, p_M, at the plane of the rotating microphones.
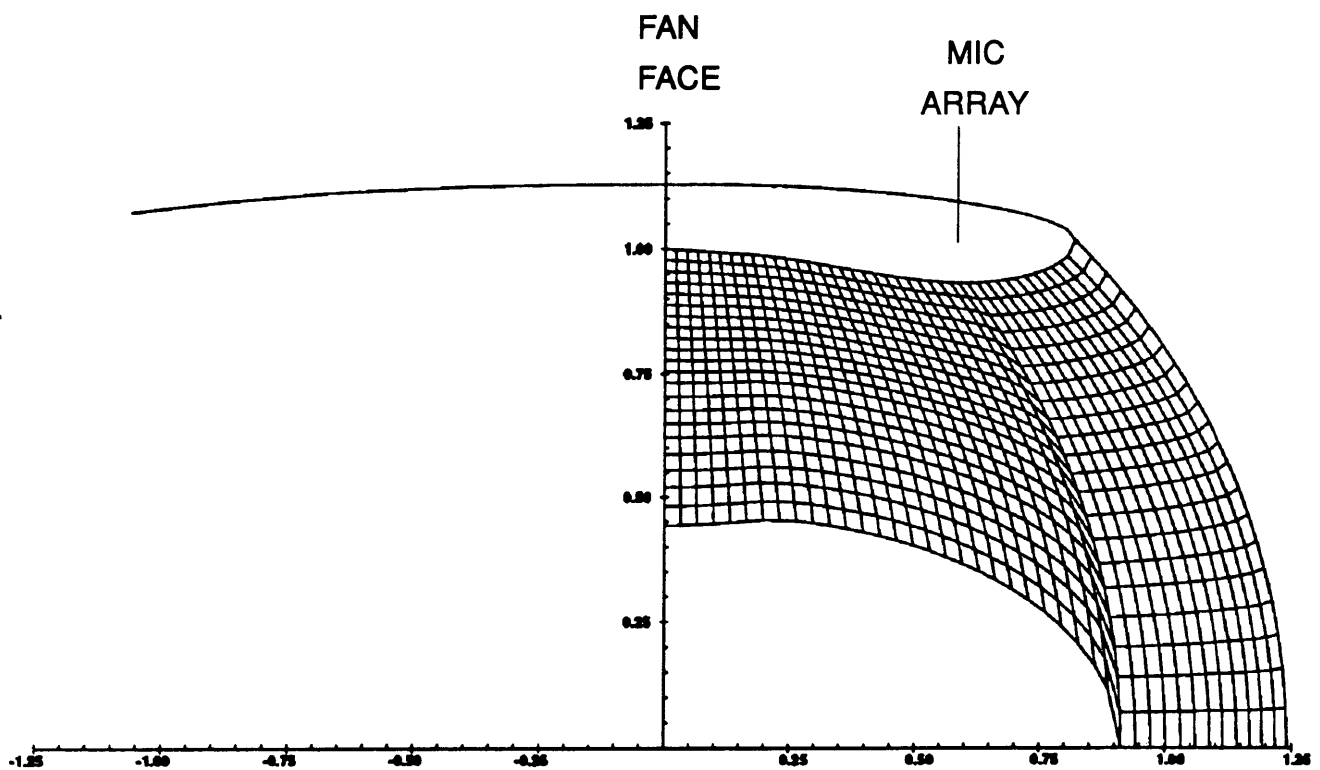
Figure 6.   Mesh system used to obtain forward waves, p_F^+, at the fan face from measured total pressures, p_M, at the plane of the rotating microphones.

$$p_M = D_{MF}\, p_F^+$$

write as $\quad p = D\, p^+$

for 3x3
$$\begin{bmatrix} p_1 \\ p_2 \\ p_3 \end{bmatrix} = \begin{bmatrix} D_{11} & D_{12} & D_{13} \\ D_{21} & D_{22} & D_{23} \\ D_{31} & D_{32} & D_{33} \end{bmatrix} \begin{bmatrix} p_1^+ \\ p_2^+ \\ p_3^+ \end{bmatrix}$$

Calibrate with successive known, unit modal inputs

first
$$\begin{bmatrix} D_{11} \\ D_{21} \\ D_{31} \end{bmatrix} = \begin{bmatrix} \bullet & & \\ \bullet & & \\ \bullet & & \end{bmatrix} \begin{bmatrix} 1 \\ 0 \\ 0 \end{bmatrix}$$
First unit input gives first column elements of D

second
$$\begin{bmatrix} D_{12} \\ D_{22} \\ D_{32} \end{bmatrix} = \begin{bmatrix} & \bullet & \\ & \bullet & \\ & \bullet & \end{bmatrix} \begin{bmatrix} 0 \\ 1 \\ 0 \end{bmatrix}$$
Second unit input gives second column of D

third
$$\begin{bmatrix} D_{13} \\ D_{23} \\ D_{33} \end{bmatrix} = \begin{bmatrix} & & \bullet \\ & & \bullet \\ & & \bullet \end{bmatrix} \begin{bmatrix} 0 \\ 0 \\ 1 \end{bmatrix}$$
Third unit input gives third column of D

Outputs from computer program are columns of D_{MF} matrix.

Figure 7.   Computer calibrations to give elements of D_{MF}.

Mode Measurement Location

16 Blade
Fan
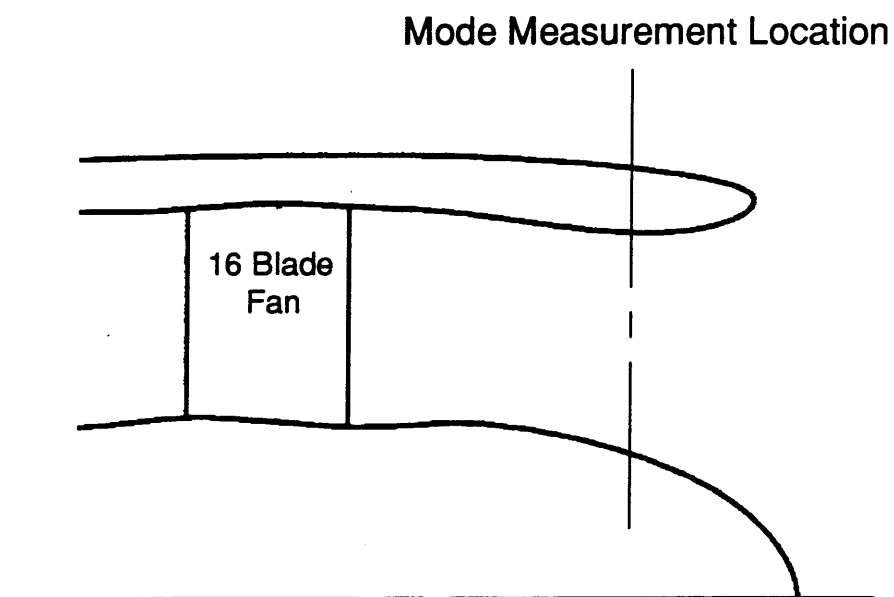
Figure 8.   Medium or mid–inlet configuration.
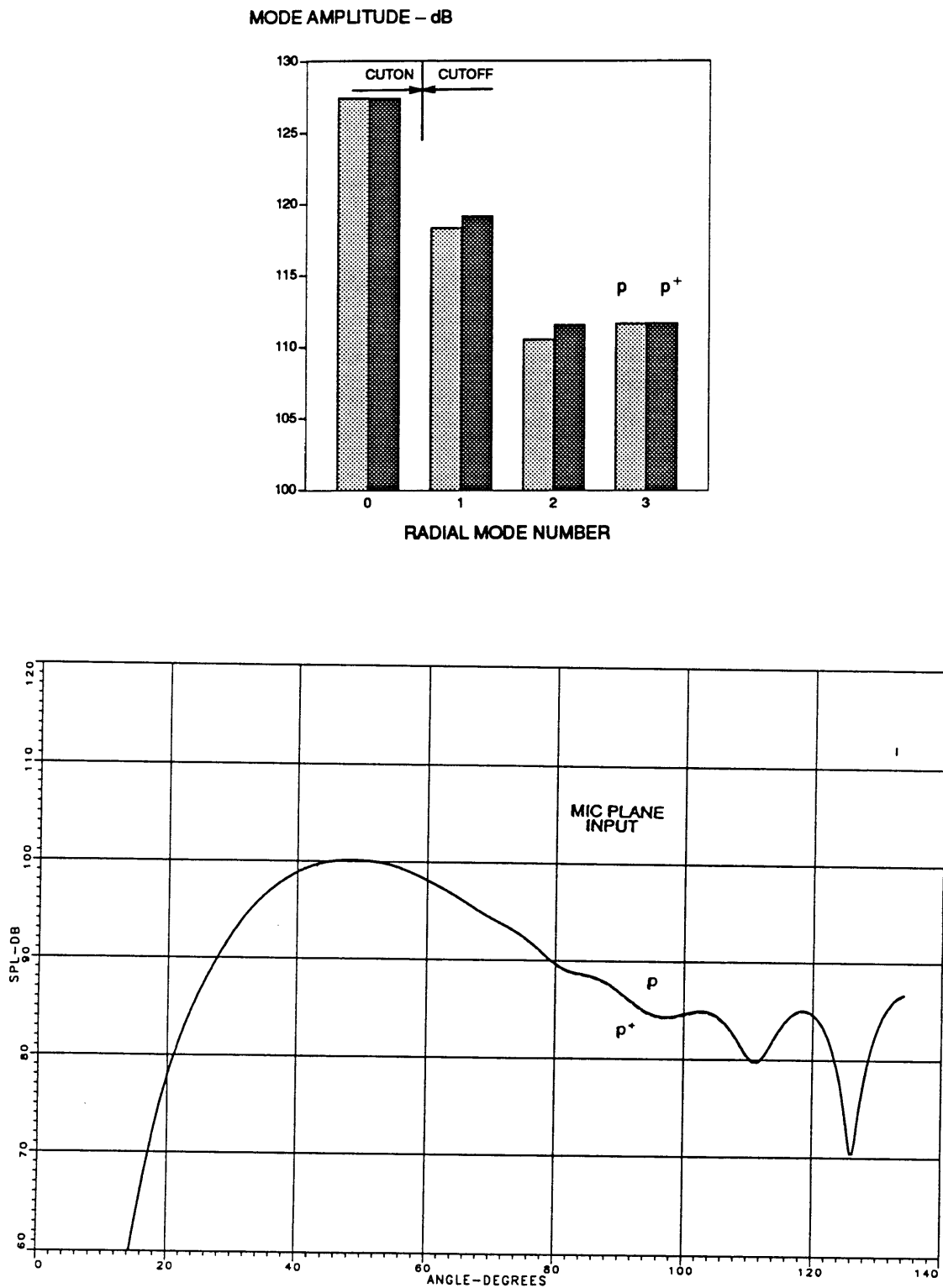
Figure 9.   Estimated far–field directivity from measured rotating microphone data.
BPF, 9600 rpm corrected rotor speed, circumferential mode = –6.
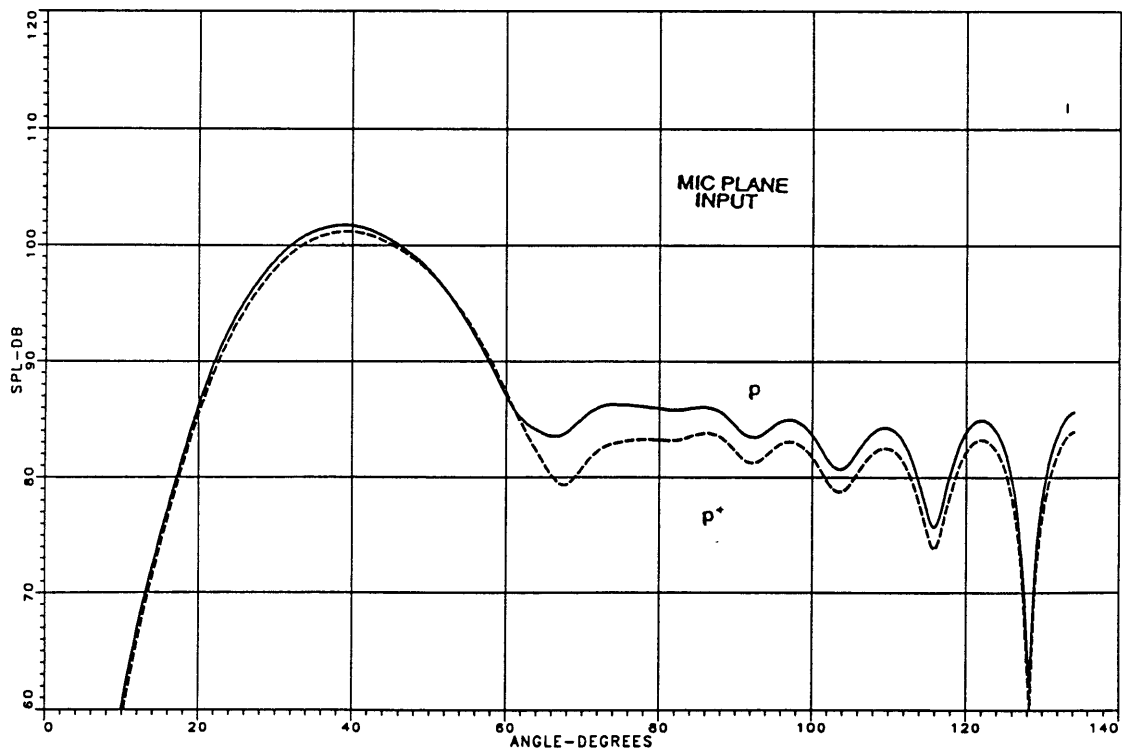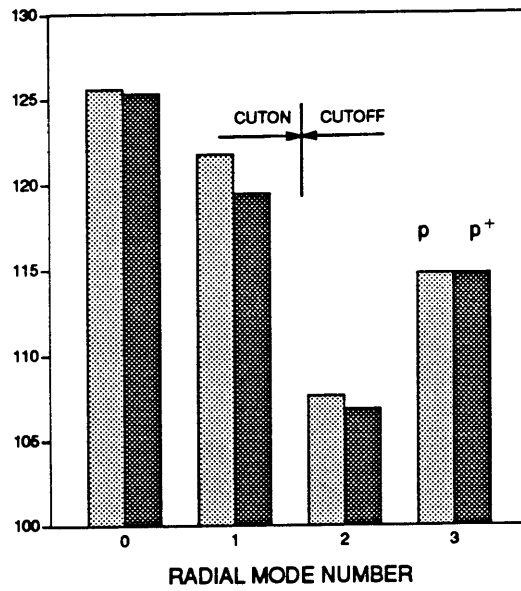
Figure 10. Estimated far–field directivity from measured rotating microphone data. BPF, 11,400 rpm corrected rotor speed, circumferential mode = –6.

MODE AMPLITUDE – dB

RADIAL MODE NUMBER
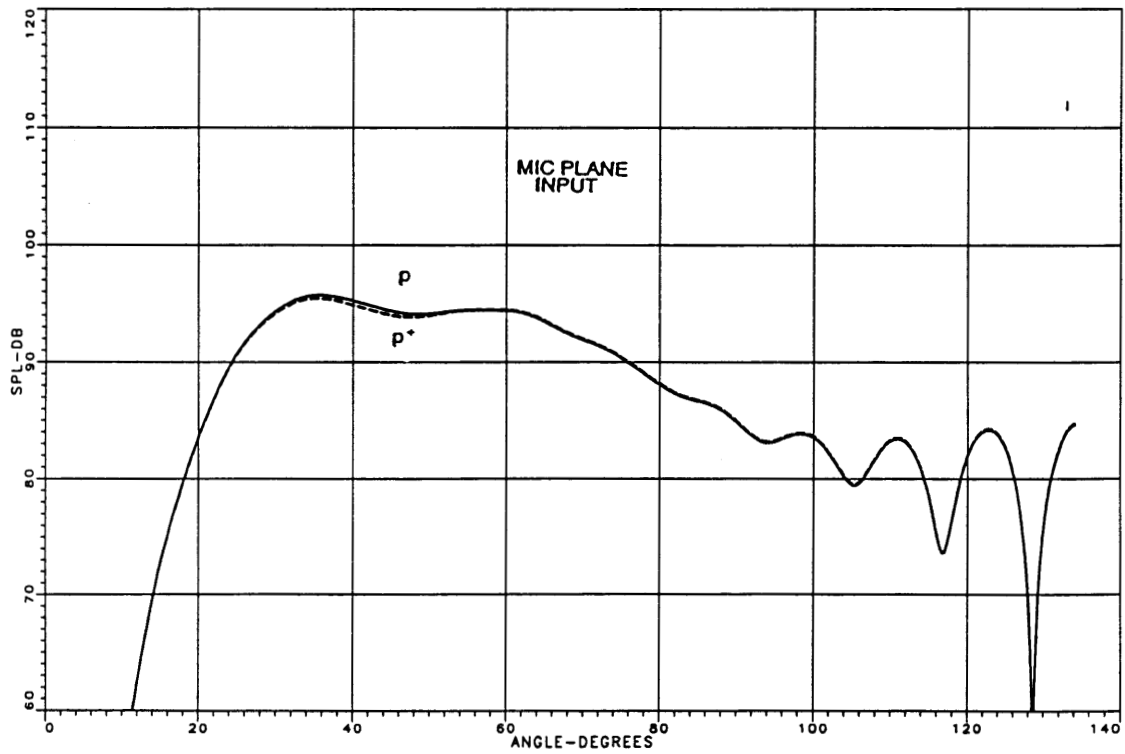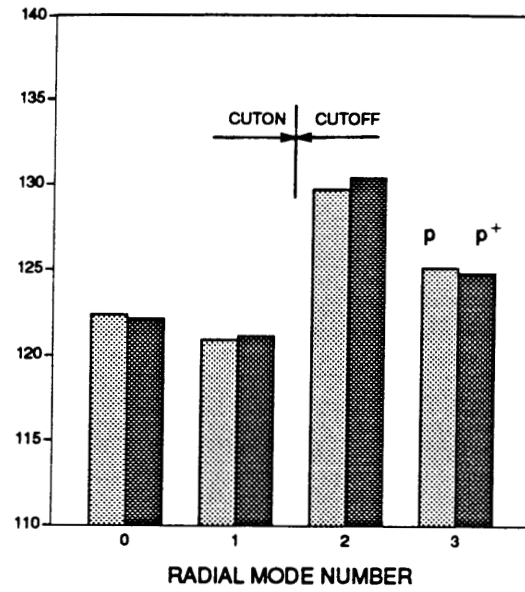
Figure 11.   Estimated far–field directivity from measured rotating microphone data.
BPF, 12,000 rpm corrected rotor speed, circumferential mode = –6.
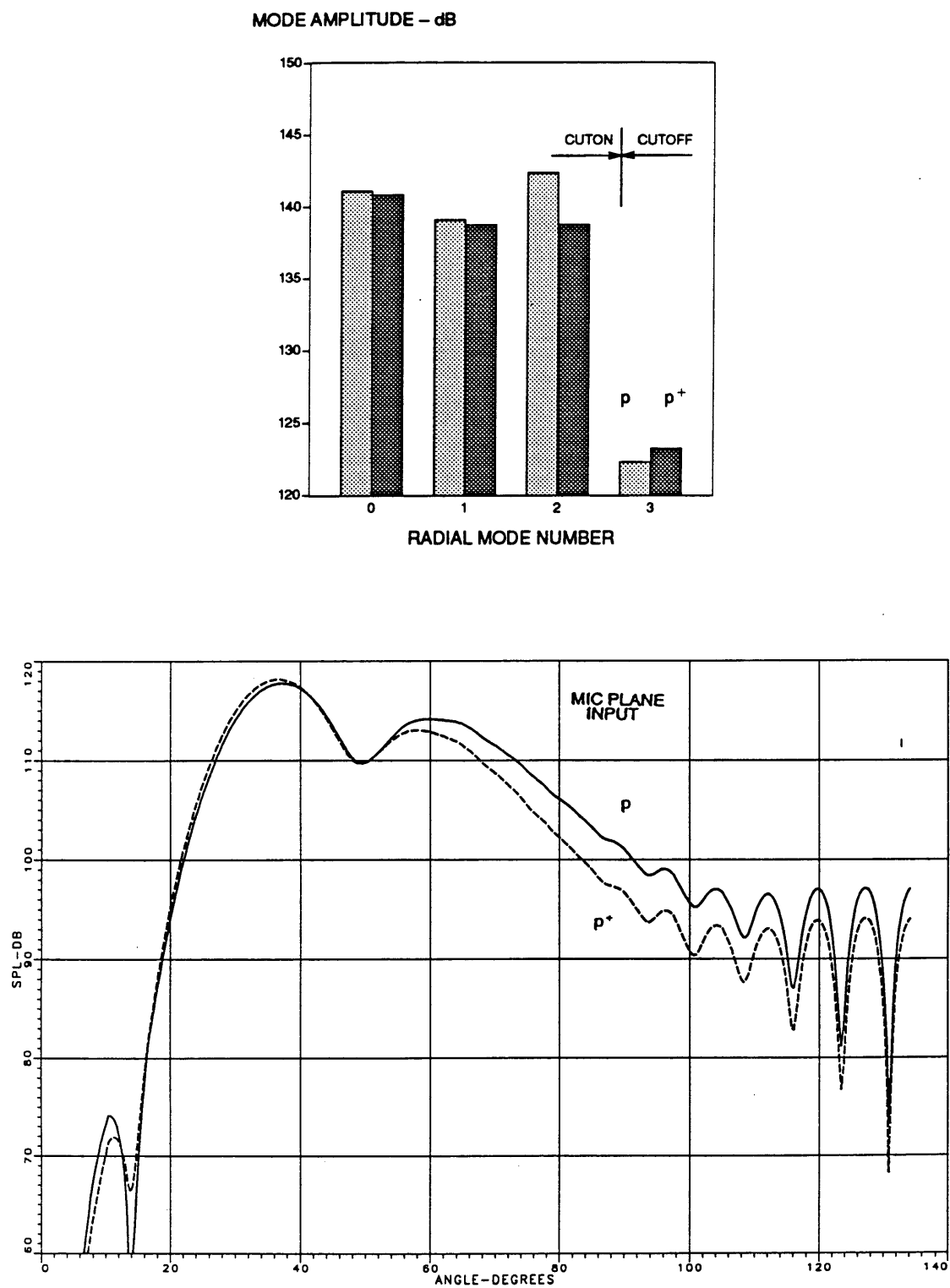
MODE AMPLITUDE — dB

Figure 12.   Estimated far–field directivity from measured rotating microphone data.
2BPF, 9,600 rpm corrected rotor speed, circumferential mode = 10.

— 45 —
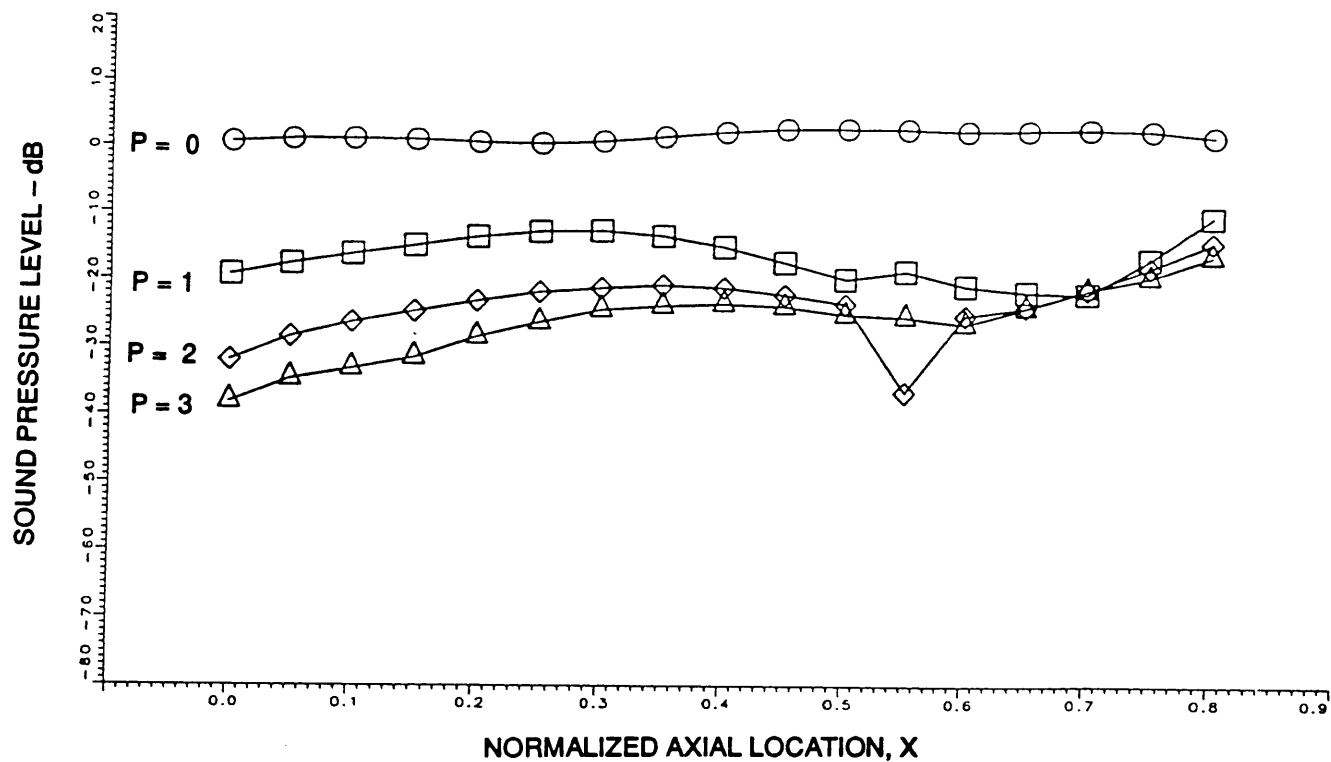
Figure 13a. Comparison of mode amplitudes, p, at various axial locations
for unit input p^+ modes. BPF = 9,600 rpm. Input $p^+ = 0$.
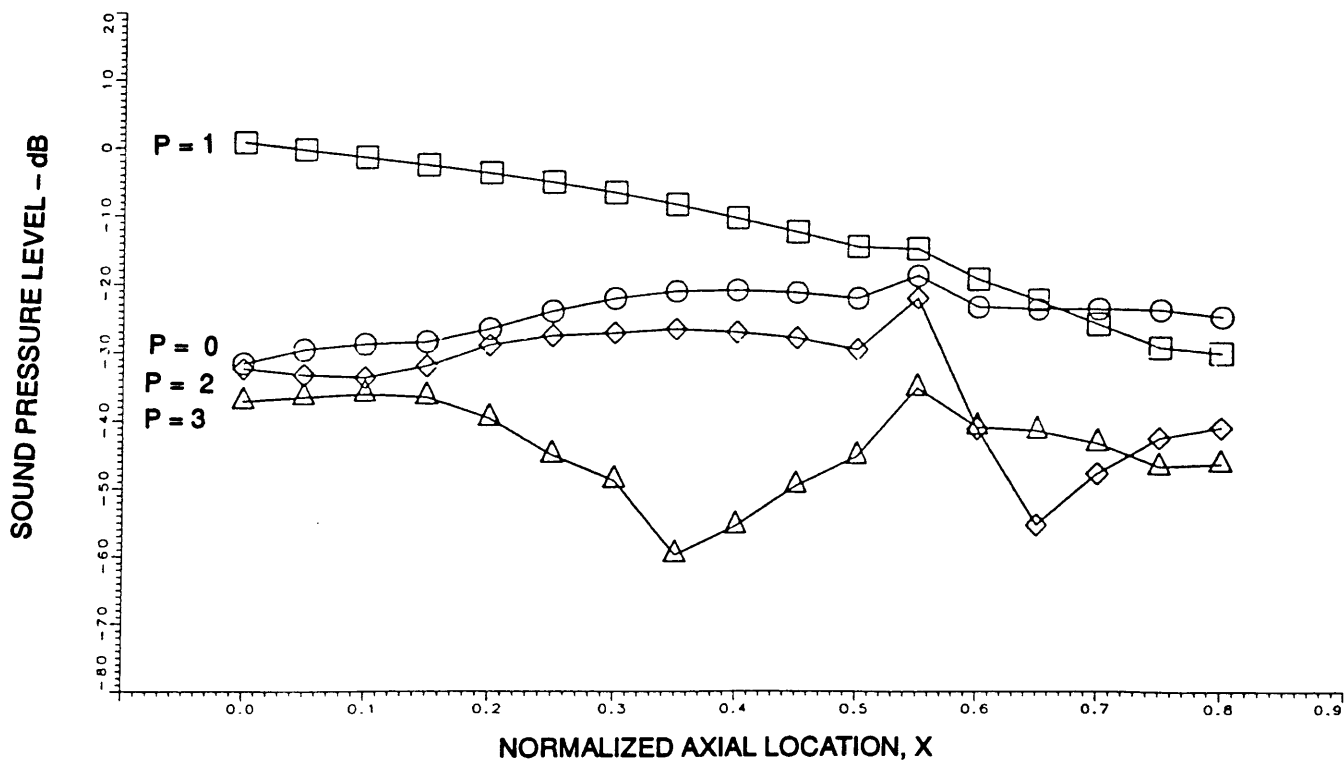
Figure 13b. Comparison of mode amplitudes, p, at various axial locations
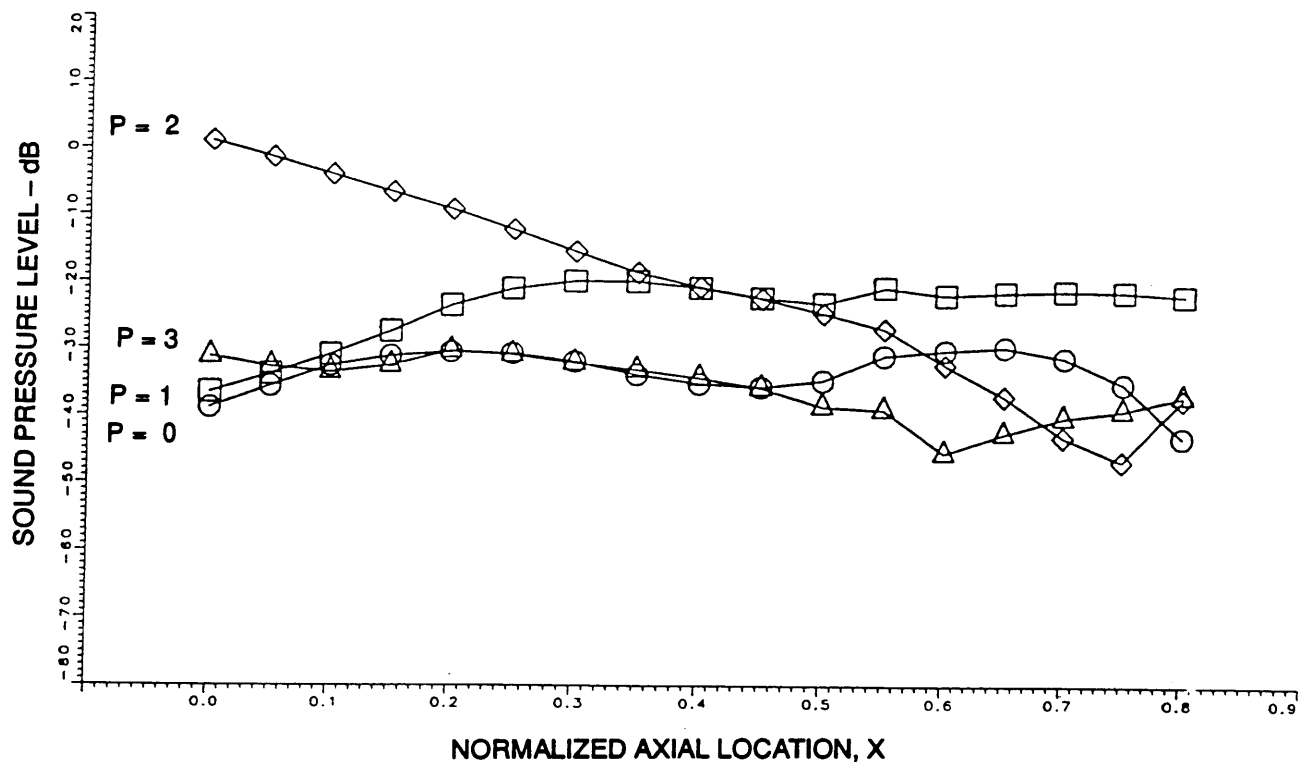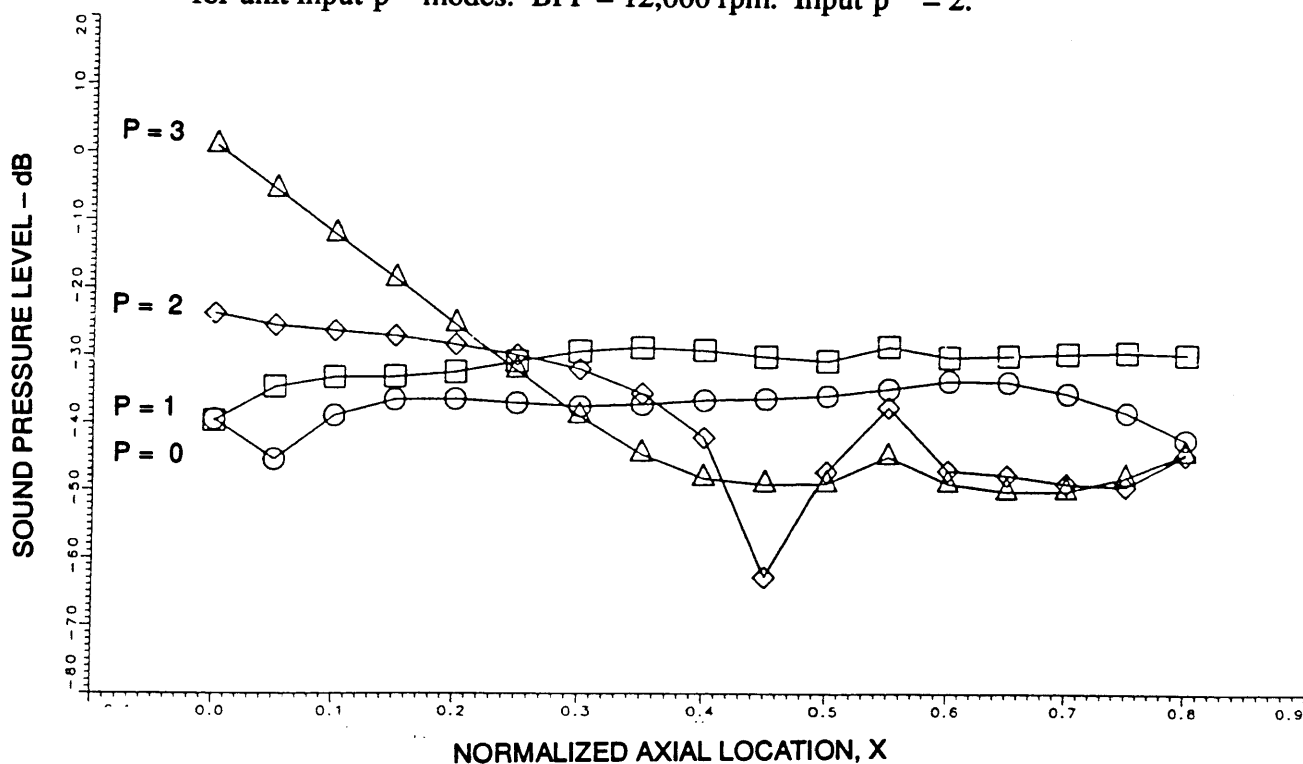for unit input p^+ modes. BPF = 9,600 rpm. Input $p_1^+ = 1$.
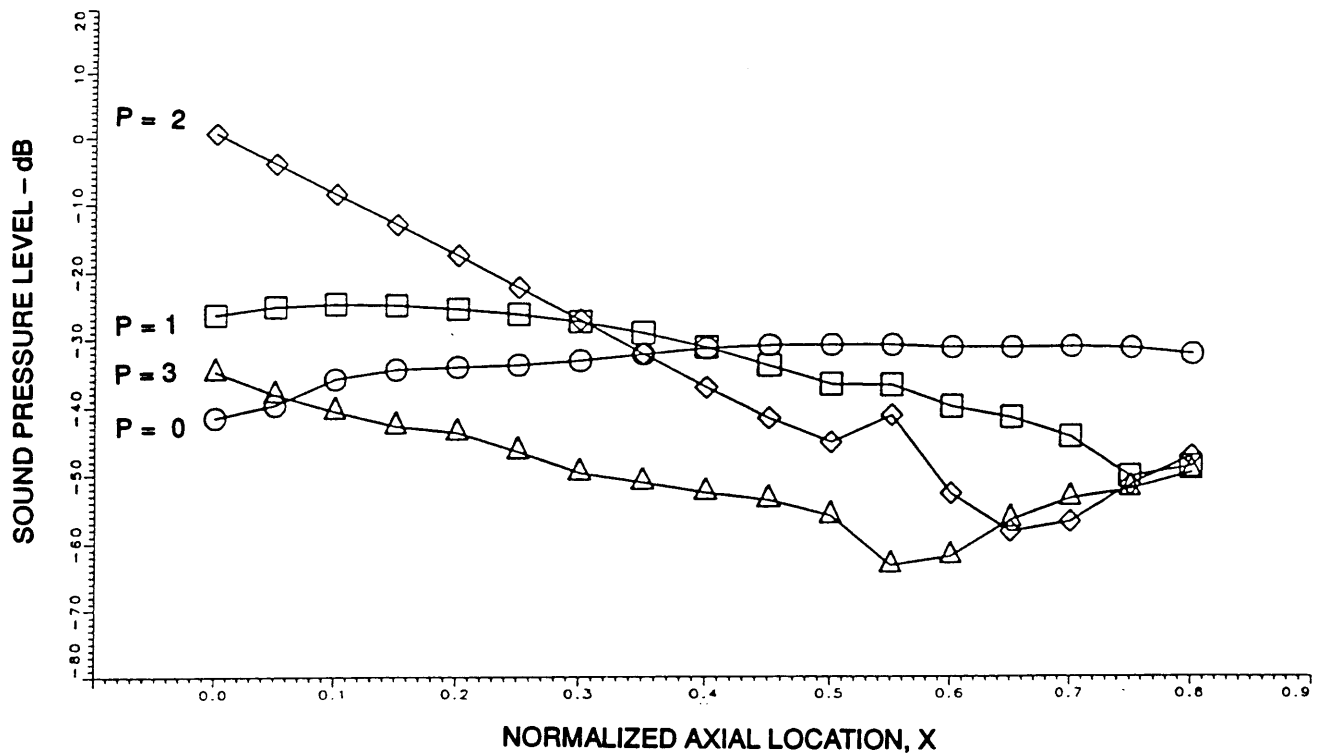
Figure 13c. Comparison of mode amplitudes, p, at various axial locations for unit input p^+ modes. BPF = 9,600 rpm. Input p^+ = 2.
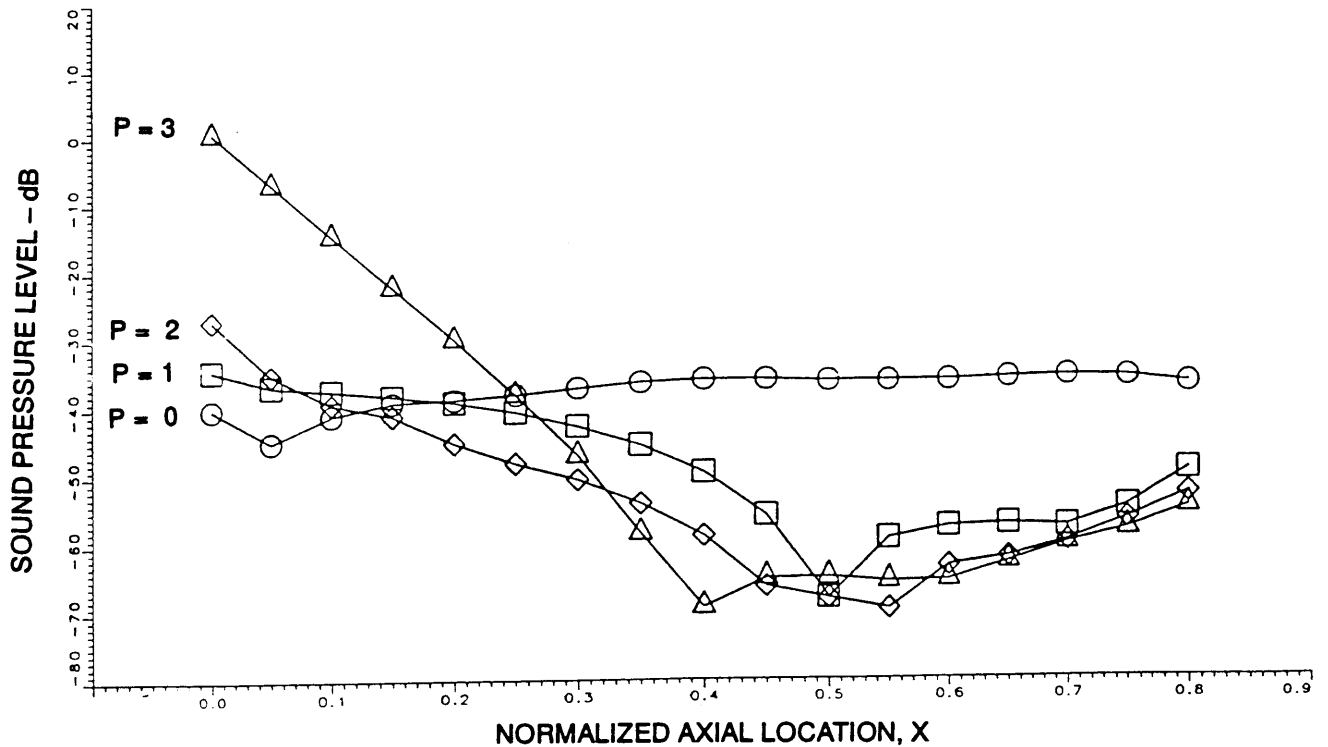
Figure 13d. Comparison of mode amplitudes, p, at various axial locations for unit input p^+ modes. BPF = 9,600 rpm. Input p_3^+ = 1.
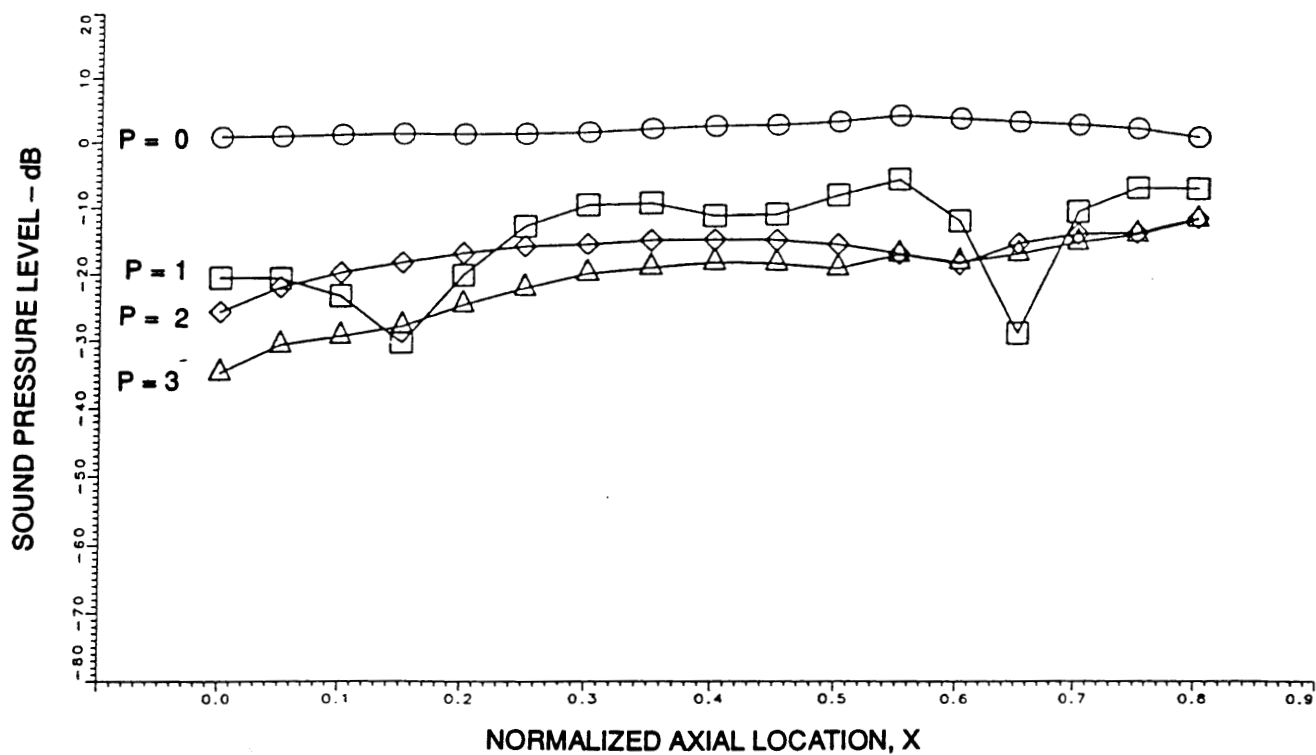
Figure 14a. Comparison of mode amplitudes, p, at various axial locations for unit input p^+ modes. BPF = 12,000 rpm. Input $p^+ = 0$.
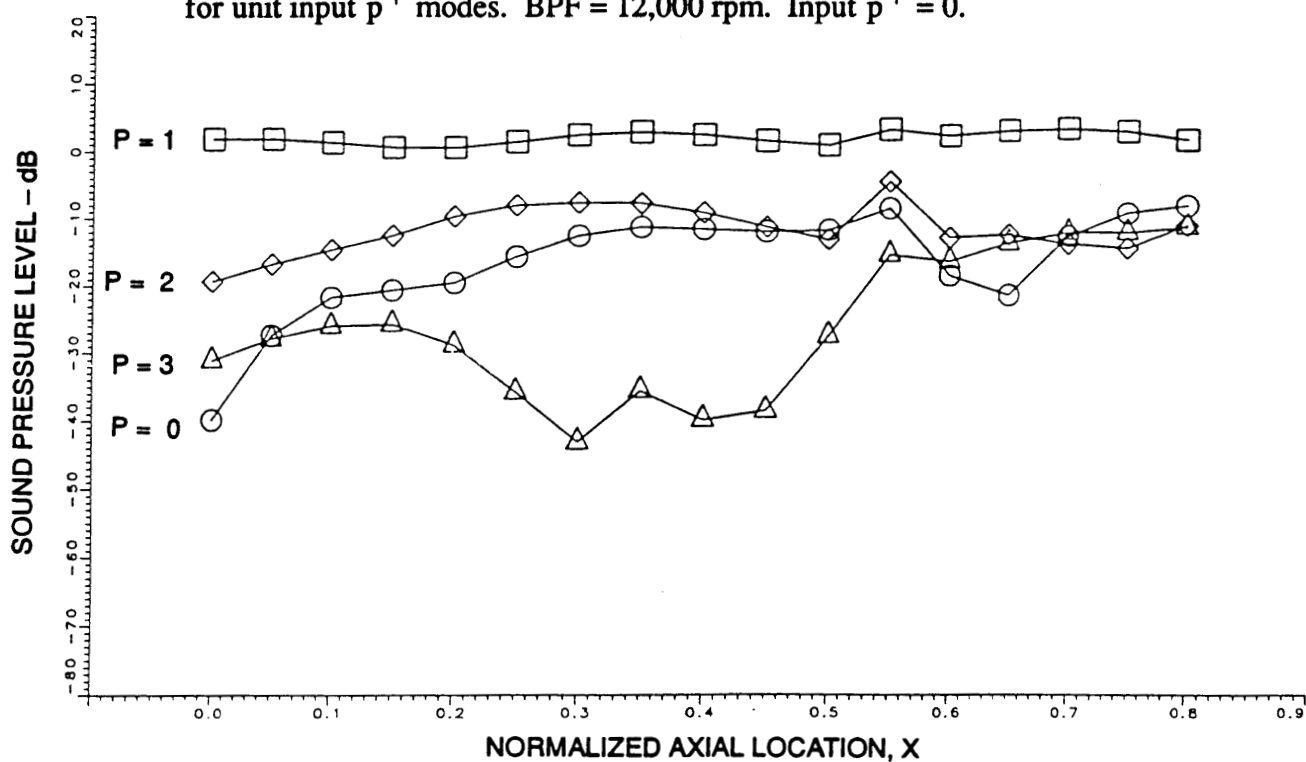
Figure 14b. Comparison of mode amplitudes, p, at various axial locations for unit input p^+ modes. BPF = 12,000 rpm. Input $p_1^+ = 1$.

Figure 14c. Comparison of mode amplitudes, p, at various axial locations for unit input p^+ modes. BPF = 12,000 rpm. Input $p^+ = 2$.

Figures 14d. Comparison of mode amplitudes, p, at various axial locations for unit input p^+ modes. BPF = 12,000 rpm. Input $p_3^+ = 1$.

REPORT DOCUMENTATION PAGE

1. AGENCY USE ONLY *(Leave blank)*	2. REPORT DATE April 1995	3. REPORT TYPE AND DATES COVERED Final Contractor Report

4. TITLE AND SUBTITLE

Method for Extracting Forward Acoustic Wave Components from Rotating Microphone Measurements in the Inlets of Turbofan Engines

6. AUTHOR(S)

D.E. Cicon and T.G. Sofrin

5. FUNDING NUMBERS

WU–538–03–11
C–NAS3–26618 Task 4

7. PERFORMING ORGANIZATION NAME(S) AND ADDRESS(ES)

UNITED TECHNOLOGIES CORPORATION
Pratt & Whitney
400 Main Street
East Hartford, Connecticut 06108

8. PERFORMING ORGANIZATION REPORT NUMBER

E–9577

9. SPONSORING/MONITORING AGENCY NAME(S) AND ADDRESS(ES)

National Aeronautics and Space Administration
Lewis Research Center
Cleveland, Ohio 44135–3191

10. SPONSORING/MONITORING AGENCY REPORT NUMBER

NASA CR–195457

11. SUPPLEMENTARY NOTES

Project Manager, Dennis L. Huff, Propulsion Systems Division, NASA Lewis Research Center, organization code 2770, (216) 433–3913.

12a. DISTRIBUTION/AVAILABILITY STATEMENT

Unclassified - Unlimited
Subject Category 07

This publication is available from the NASA Center for Aerospace Information, (301) 621–0390.

12b. DISTRIBUTION CODE

13. ABSTRACT *(Maximum 200 words)*

This report describes a procedure for enhancing the use of the basic rotating microphone system so as to determine the forward propagating mode components of the acoustic field in the inlet duct at the plane of the microphone plane in order to predict more accurate far-field radiation patterns. In addition, a modification was developed to obtain, from the same microphone readings, the forward acoustic modes generated at the fan face, which is generally some distance downstream of the microphone plane. Both these procedures employ computer-simulated calibrations of sound propagation in the inlet duct, based upon the current radiation code. These enhancement procedures were applied to previously obtained rotating microphone data for the 17–inch ADP fan. The forward mode components at the microphone plane were obtained and were used to compute corresponding far-field directivities. The second main task of the program involved finding the forward wave modes generated at the fan face in terms of the same total radial mode structure measured at the microphone plane. To obtain satisfactory results with the ADP geometry it was necessary to limit consideration to the propagating modes. Sensitivity studies were also conducted to establish guidelines for use in other fan configurations.

14. SUBJECT TERMS

Fan acoustics mode measurements; Rotating microphone

15. NUMBER OF PAGES
52

16. PRICE CODE
A04

17. SECURITY CLASSIFICATION OF REPORT	18. SECURITY CLASSIFICATION OF THIS PAGE	19. SECURITY CLASSIFICATION OF ABSTRACT	20. LIMITATION OF ABSTRACT
Unclassified	Unclassified	Unclassified	